Author Manuscript

Author Manuscript

Author Manuscript

Author Manuscript

HHS Public Access

Author manuscript

Neurobiol Dis. Author manuscript; available in PMC 2017 July 01.

Published in final edited form as:

Neurobiol Dis. 2016 July ; 91: 166–181. doi:10.1016/j.nbd.2016.03.003.

Aberrant excitatory rewiring of layer V pyramidal neurons early after neocortical trauma

D. Koji Takahashi, **Feng Gu Isabel**, **Shri Vyas Parada**, and **David A. Prince**

Epilepsy Research Laboratories, Department of Neurology and Neurological Sciences, Stanford University School of Medicine, Stanford, California 94305

Abstract

Lesioned neuronal circuits form new functional connections after a traumatic brain injury (TBI). In humans and animal models, aberrant excitatory connections that form after TBI may contribute to the pathogenesis of post-traumatic epilepsy. Partial neocortical isolation ("undercut" or "UC") leads to altered neuronal circuitry and network hyperexcitability recorded in vivo and in brain slices from chronically lesioned neocortex. Recent data suggest a critical period for maladaptive excitatory circuit formation within the first 3 days post UC injury (Graber and Prince, 1999, 2004; Li et al., 2011, 2012b). The present study focuses on alterations in excitatory connectivity within this critical period. Immunoreactivity (IR) for growth-associated protein (GAP)-43 was increased in the UC cortex 3 days after injury. Some GAP-43-expressing excitatory terminals targeted the somata of layer V pyramidal (Pyr) neurons, a domain usually innervated predominantly by inhibitory terminals. Immunocytochemical analysis of pre- and postsynaptic markers showed that putative excitatory synapses were present on somata of these neurons in UC neocortex. Excitatory postsynaptic currents from UC layer V Pyr cells displayed properties consistent with perisomatic inputs and also reflected an increase in the number of synaptic contacts. Laser scanning photostimulation (LSPS) experiments demonstrated reorganized excitatory connectivity after injury within the UC. Concurrent with these changes, spontaneous epileptiform bursts developed in UC slices. Results suggest that aberrant reorganization of excitatory connectivity contributes to early neocortical hyperexcitability in this model. The findings are relevant for understanding the pathophysiology of neocortical post-traumatic epileptogenesis and are important in terms of the timing of potential prophylactic treatments.

Keywords

neocortex; traumatic brain injury; excitatory synapses; excitatory circuits; EPSCs; laser scanning photostimulation; epileptogenesis; pyramidal cells; VGLUT1; PSD95

Corresponding author: David Prince, M.D. daprince@stanford.edu, 300 Pasteur Dr. SUMC RM M016, Stanford, CA 94305-5122, Phone: 650-723-5522, Fax: 650-723-1080.

Conflict of Interest: None to declare.

Authors contributions: DKT, DAP planned the experiments and wrote the ms; DKT, FG collected and analyzed electrophysiological data; IP, SV performed and analyzed the immunocytochemistry.

Publisher's Disclaimer: This is a PDF file of an unedited manuscript that has been accepted for publication. As a service to our customers we are providing this early version of the manuscript. The manuscript will undergo copyediting, typesetting, and review of the resulting proof before it is published in its final citable form. Please note that during the production process errors may be discovered which could affect the content, and all legal disclaimers that apply to the journal pertain.

Author Manuscript Author Manuscript Author Manuscript Author Manuscript

Introduction

Injury to the central nervous system initiates a variety of changes including gliosis, inflammation, and reorganization of neural circuitry. For example, in animal models of axotomy (Fishman and Mattu, 1993), diffuse axonal injury (Greer et al., 2011) and cortical stab wounds (King et al., 2001), injury is accompanied by axonal sprouting. Ramon ý Cajal, perhaps the first to observe this phenomenon, referred to rapid axonal sprouting after injury as “compensatory collateral hypertrophy” and hypothesized that it was a mechanism to rewire lesioned cortical circuits (DeFelipe and Jones, 1991). Reorganization after injury can be adaptive if lost connections in vacant synaptic territory are re-established (Carmichael, 2003; Chuckowree et al., 2004), or maladaptive, for example, if aberrant and excessive excitatory connections initiate epileptogenesis (Salin et al., 1995; McKinney et al., 1997; Jin et al., 2006).

Traumatic brain injury (TBI) accounts for ~20% of all symptomatic epilepsies, making it one of the most common forms of acquired epilepsy worldwide (Hauser et al., 1991; Kraus and McArthur, 1996; Herman, 2002). Key risk factors for the development of epilepsy after TBI include penetrating brain injuries, depressed skull fracture, intracranial hematoma, and the occurrence of acute symptomatic seizures (i.e. “early seizures”) within the first week (Frey, 2003; Lowenstein, 2009; Beghi et al., 2010). Partial neocortical isolations provide a model of focal TBI in which mechanisms of hyperexcitability after injury can be examined (Prince and Tseng, 1993; Hoffman et al., 1994; Salin et al., 1995; Topolnik et al., 2003a). In slices obtained from chronically injured animals weeks to months after injury, robust epileptiform activity is observed in layer V of neocortex (Prince and Tseng, 1993; Hoffman et al., 1994; Li and Prince, 2002). Similar to other animal models of post-traumatic epileptogenesis (D’Ambrosio et al., 2004; Cohen et al., 2007; Avramescu et al., 2009), hyperexcitability in the UC neocortex is hypothesized to originate from enhanced excitation (Salin et al., 1995; Li and Prince, 2002; Jin et al., 2006) and decreased inhibition (Li and Prince, 2002; Avramescu et al., 2009; Faria and Prince, 2010; Jin et al., 2011; Faria et al., 2012; Ma and Prince, 2012). The present experiments were motivated by recent data suggesting a critical period of maladaptive excitatory circuit formation within the first 3 days following UC (Graber and Prince, 1999, 2004; Li et al., 2011, 2012b). We used anatomical, electrophysiological, and laser photolysis methods to assess acute changes in excitatory circuits. Results show that markers of axonal sprouting of excitatory terminals are present in cortical slices 3 days after UC, concomitant with spontaneous epileptiform activity. Our results also suggest that some newly sprouted excitatory axon terminals aberrantly target the perisomatic region of layer V Pyr neurons, as evidenced by immunocytochemical data, larger and faster spontaneous excitatory post synaptic currents (sEPSCs), and a negatively shifted reversal potential for evoked glutamate-receptor mediated currents. Finally, laser scanning experiments demonstrate larger amplitude EPSCs terminating on layer V Pyr neurons in UC slices. The results suggest that aberrant excitatory inputs to layer V Pyr neurons develop soon after injury and could contribute to early neocortical hyperexcitability in this model of traumatic brain injury and early seizures after TBI in humans.

Author Manuscript Author Manuscript Author Manuscript Author Manuscript

Materials and Methods

Partial cortical isolations

All experiments were performed according to the National Institutes of Health guide for the care and use of Laboratory animals and all protocols were approved by the Stanford Institutional Animal Care and Use Committee. Partial isolations of neocortex ("UCs") were produced in anesthetized male rats at postnatal day 21 (P21, P0 = date of birth) as described previously (Hoffman et al., 1994; reviewed in Graber and Prince, 2006). Briefly, animals were deeply anesthetized with ketamine (80 mg/kg, ip) and xylazine (8 mg/kg, ip) and mounted in a stereotactic frame. A cranial bone window (~ 3 x 5 mm) centered on the coronal suture was removed, leaving the dura intact, to expose a portion of the frontoparietal cortex. A 30-gauge needle bent at a right angle 3 mm from the tip was inserted parasagitally ~1–2 mm from the central sulcus with the needle point aimed rostrally. The needle was advanced tangentially through the dura and pia, just beneath the pial vessels, and lowered to a depth of 2 mm. The needle was then rotated on its longitudinal axis by ~120° – 180° to produce a contiguous white matter lesion. The needle was then elevated to a position just under the pia to make a second transcortical cut and removed. The skull opening was covered with sterile Saran Wrap® and the skin sutured. The animals were then allowed to recover in a temperature- and light-controlled (12 h light/dark cycle) environment with access to food and water ad libitum until the terminal experiment.

Slice preparation and electrophysiology

Acute neocortical brain slices were prepared from UC animals 3 – 4 days after injury (referred to below as 3 day UC group) and from age-matched male littermates. "Control" below refers to age matched naïve littermates, unless otherwise noted. Animals were deeply anesthetized with sodium pentobarbital (55 mg/kg, i.p.), brains rapidly removed and placed in ice-cold (4°C) sucrose artificial cerebrospinal fluid cutting solution (sACSF) containing (in mM): 234 sucrose, 26 $NaHCO_3$, 11 glucose, 10 $MgSO_4$, 2.5 KCl, 1.25 NaH_2PO_4, and 0.5 $CaCl_2$ gassed with 95% O_2/5% CO_2. Brains were then blocked and mounted on a vibratome stage (VT 1200, Leica). Coronal brain slices (300 μm) containing the sensorimotor cortex (the region of injury in UC animals) were cut in oxygenated sACSF and immediately transferred to an incubation chamber filled with oxygenated artificial cerebrospinal fluid (ACSF) containing (in mM): 126 NaCl, 26 $NaHCO_3$, 10 glucose, 2.5 KCl, 1.25 NaH_2PO_4, 2 $CaCl_2$, and 1 $MgSO_4$; osmolarity 295–300 mOsm, pH 7.4 when gassed with 95% O_2/5% CO_2. Slices were incubated at 34°C for 1 h and then at room temperature until they were transferred to the recording chamber. The undercut cortical area was clearly visible and recordings were made from layer V within the UC 1–2 mm from the transcortical cuts. Earlier results identified this area as the site of onset of epileptiform bursts (Prince and Tseng, 1992; Hoffman et al, 1994).

Patch electrodes were pulled from borosilicate glass (1.5 mm OD, Sutter Instruments) and had an impedance of 3 – 5 M when filled with an internal solution containing (in mM): 130 Cs-gluconate, 8 CsCl, 10 HEPES, 4 EGTA, 2 NaCl, and 10 N-ethyllidocaine chloride (QX314, Tocris). 0.5% biocytin was also included in the internal solution for later

Author Manuscript Author Manuscript Author Manuscript Author Manuscript

visualization of the recorded cell. The osmolarity of the internal solution was adjusted to 290–295 mOsm with double distilled water and the pH to 7.35 – 7.4 with CsOH.

Whole-cell voltage clamp recordings were made from minimally submerged brain slices in a custom built recording chamber. Cells were visualized using infrared differential interference contrast (IR-DIC) microscopy (Zeiss Akioskop, Carl Zeiss) and a 63x water immersion lens (Achroplan 63x, 0.9W, Carl Zeiss). Layer V Pyr neurons were identified as neurons with pyramidal shaped somata and a single emerging dendrite extending toward the pial surface. Post hoc biocytin immunohistochemistry was used to positively identify recorded control neurons and cells from UC cortex as pyramidal. Recordings were obtained with a Multiclamp 700A amplifier and Clampex 9 software interfaced to a Digidata 1322A 16-bit data acquisition board (Molecular Devices). Signals were sampled at 10 kHz and low pass filtered at 4 kHz. Holding potential was corrected for a calculated 13 mV liquid junction potential. All recordings were obtained at 32° C with gravity fed oxygenated solutions at a minimum flow rate of 3.5 ml/min.

Analysis of postsynaptic currents

Recordings were obtained from control slices (n = 29 cells from 14 animals, R_s: 18.9 ± 1 MΩ) and UC slices 3 days after injury (n = 23 cells from 13 UC animals, R_s: 18.1 ± 1.4 MΩ). Only continuous stable recordings with less than 15% drift in R_s were used for analysis. EPSCs were analyzed from 2 – 6 minutes of recording. EPSCs were recorded at a holding potential (V_h) of −65 mV, the estimated E_{Cl^-} with the Cs-gluconate internal solution, unless otherwise noted. Miniature excitatory post synaptic currents (mEPSCs) were recorded in the presence of 1 μM TTX. EPSCs were detected and analyzed with MiniAnalysis (Synaptosoft) and Matlab (MathWorks).

Spontaneous activity in UC slices was composed of both EPSCs and epileptiform activity, defined as prolonged (>100 ms) bursts of EPSCs. Therefore, to assess the frequency and kinetics of EPSCs, care was taken to analyze only events that occurred outside of the epileptiform bursts. Only one Pyr cell was recorded from each slice. Only EPSCs with clearly measureable baselines, peaks, and decay times with smooth rising and falling phases were measured. Rise times were defined as the time from 10% to 90% of peak amplitude calculated from baseline. Cumulative distributions of EPSC kinetics (amplitude, rise time, half widths) were analyzed by randomly selecting 50 sEPSCs per cell, and significance of differences determined with Kolmogorov-Smirnov (KS) tests. The same randomly-selected sample was used for scatter plots (see below).

mEPSCs were obtained in a similar manner from control (n = 11 cells from 3 animals, R_s: 13.1 ± 1.1 MΩ) and UC animals 3 days after injury (n = 9 cells from 3 animals, R_s: 12.9 ± 1.2 MΩ). To compare cumulative distributions of mEPSC kinetics and to construct mEPSC scatter plots, in a similar manner to sEPSC analysis described above, 50 events were randomly selected per cell for data analysis.

Epileptiform bursts were distinguished from sEPSCs using a custom routine written in Matlab. Using a threshold criterion, 10 or more consecutive EPSCs occurring with inter-event intervals less than 25 ms were identified as putative bursts. Visual examination of

Author Manuscript Author Manuscript Author Manuscript Author Manuscript

recordings confirmed the accuracy of this method for automated burst detection, and the methodology was subsequently applied with identical analysis parameters to all recordings from control and UC animals. Therefore, the number of epileptiform bursts per minute and the cumulative amplitude of synaptic activity during epileptiform bursts were quantified using this analysis method and sEPSCs could be analyzed independent of bursting activity.

The cloud density analysis algorithm was based on “Scattercloud” by Steve Simon (MathWorks). Cloud density analysis was used to find differences in the density of massively overlapping scatter data. Regional differences in density were determined with a two-dimensional histogram using 50 equally spaced bins in the X and Y axis. The number of events in each bin was counted and a color coded and smoothed surface was then fit to this data. The peak of the surface corresponds to the bin with the greatest number of events. To ensure equal representation of data, the same randomly chosen samples used in cumulative distributions were used for scatter analysis (i.e. scatter plots were made from 50 events randomly chosen per cell, see above). Identical binning and smoothing parameters were used to compare control and experimental data.

Glutamate receptor mediated reversal potentials

In experiments focused on the α-amino-3-hydroxy-5-methyl-4-isoxazolepropionic acid (AMPA) receptor-mediated reversal potentials, extracellular stimulation was delivered with an ACSF-filled theta glass pipette (<1.5 μm tip) positioned ~20 μm from the soma of the recorded cell. For these experiments, gabazine (10 μM) and D-(-)-2-Amino-5-phosphonopentanoic acid (D-APV, 100 μM) were added to the bath to block gamma-aminobutyric acid ($GABA_A$) and N-methyl-D-aspartate (NMDA) receptors, respectively. In order to standardize stimulus parameters between cells, for each experiment, stimulus duration was first varied in step-wise fashion from 1–100 μs, in increments of 10 μs, while holding the cell at V_h = −65mV, until the first reliable postsynaptic response above threshold was detected. This stimulus intensity was then fixed for a given cell/experiment to evoke postsynaptic currents. Layer V Pyr cells were voltage clamped to V_h ranging from −73 mV to + 47 mV (corrected for a 13 mV liquid junction potential) in incremental steps of 20 mV. EPSCs were evoked after holding the cell at a given membrane potential for a minimum of 4 seconds. Voltage-gated calcium currents were occasionally observed at depolarized holding potentials but were inactivated after several hundred milliseconds. Two to four evoked EPSCs were averaged at each V_h, the peak values normalized on a per cell basis, and a linear regression curve fit through the data points to obtain I-V relationships and to calculate reversal potentials.

Laser Scanning Photostimulation (LSPS)

LSPS of caged glutamate was performed as described previously (Deleuze and Huguenard, 2006; Jin et al., 2006, 2011). Briefly, slices were submerged in a recording chamber at room temperature and perfused with 20 ml of re-circulating ACSF containing a high divalent cation concentration (4mM Ca^{2+} / 4mM Mg^{2+}), 20 μM D-APV (to block NMDA receptors), and 100 μM 4-Methoxy-7-nitroindolinyl-caged-L-glutamate (MNI-caged-L-glutamate, Tocris). The high divalent cation content, combined with APV, was used to reduce spontaneous epileptiform activity and recurrent polysynaptic excitation (Shepherd et al.,

Author Manuscript Author Manuscript Author Manuscript Author Manuscript

2003; Jin et al., 2006). Layer V Pyr neurons from slices of control (n = 14 cells from 5 animals, R_s = 13.6 ± 1.3 MΩ) and UC (n = 17 cells from 8 animals, R_s = 16.5 ± 1.2 MΩ) were recorded at room temperature with a potassium gluconate internal solution that contained (in mM): 130 K-gluconate, 10 KCl, 10 HEPES, 10 EGTA, 3 ATP-Mg, 0.3 GTP-Na (pH 7.40, 295 mOsm).

A frequency-tripled Nd:YVO_4 laser (Series 3500 pulsed laser, 100 kHz repetition rate, DPSS Lasers) delivered 500 mW of 355 nm light. The beam was directed through the epifluorescent port of the microscope, steered precisely in XY space by galvanometer controlled mirrors (model 6210H, Cambridge Technology), and beam expanded 2x to underfill the back aperture of a 5x Fluar objective (0.25 NA, Zeiss). Beam diameter at the back aperture was approximately 2 mm with a power density of ~40 mW/mm^2. The optical path through the objective resulted in a Gaussian beam with a theoretical waist width (W_0) of ~7.4 μm and a depth of focus of ~245 μm at the focal plane. The UV laser was Q-switched to provide a 100–300 μs “flash” of uncaging light per stimulus. Stimulus locations were separated by 75 μm. To prevent glutamate toxicity, local caged-glutamate depletion, and/or receptor desensitization, stimulus locations were visited randomly and without consecutive stimulation in any one quadrant (Shepherd et al., 2003). Custom software and hardware developed by John Huguenard and Carl Pisaturo (Deleuze and Huguenard, 2006; Jin et al., 2006) was used to direct and trigger the laser during data acquisition. To normalize uncaging stimuli between cells, glutamate was uncaged directly onto the soma of the recorded cell with a small 5x5 grid (50 μm spacing) and the laser duration was adjusted so that the maximal peak current for any directly evoked (non-synaptic) event was ~300 pA for each cell.

The data generated from LSPS, the recorded electrophysiological traces and corresponding stimulus locations (in xy coordinates) were analyzed with Matlab. A peak detection algorithm based on the cumulative derivative function (Cohen and Miles, 2000) was applied to a filtered trace to find downward peaks and their onset (i.e. when the current deflected in the downward direction). Each trace was normalized to a baseline 50 ms before laser onset. Peak detection was restricted to the first 75 ms following laser stimulation. This time window was determined empirically from the excitation profile of layer V Pyr cells recorded under cell-attached conditions (Shepherd et al., 2003). The following restrictions were made on analyzed currents: directly evoked currents (i.e. from glutamate uncaged directly on to the recorded cell) were defined as having an onset within 3 ms of the laser stimulus; putative evoked monosynaptic currents occurred with onsets after 3 ms and during the 75 ms analysis window. An interactive data analysis script allowed the user to click on each stimulus location, observe the recorded and analyzed current, and verify that analysis parameters were accurately detecting events for any given experiment.

The maximal peak amplitude of putative monosynaptic EPSCs evoked by LSPS stimulation was displayed as a heat map in relation to the location of the recorded cell. 3–5 maps were obtained from each cell using identical stimulus, map, and data analysis parameters (laser intensity, grid spacing, detection windows, peak threshold criteria, etc). If an event was evoked from the same location (i.e. “hot spot”) in more than one map, the peak amplitude across trials was used to create a single composite peak amplitude heat map. For visualizing

Author Manuscript Author Manuscript Author Manuscript Author Manuscript

data across cells (i.e. the data across multiple composite maps), the surface of each map was interpolated onto an “ideal map” spanning the full extent of the sampled region, essentially binning the data to 50 μm “blocks”. Maps were then registered to one another based on the location of the recorded cell and laminar orientation and summed to visualize all hot spots of connectivity. To quantify differences in the number of large amplitude events, the total number of hot spots greater than 100 pA was divided by the number of maps sampled and in a separate analysis, by the number of grid locations sampled. Significance was determined by Chi-square test.

Immunocytochemistry

Perfusion fixation: Rats were deeply anesthetized with B-euthanasia (100 mg/kg ip) and transcardially perfused with 4 % paraformaldehyde. Brains were dissected and cryoprotected. 40 μm coronal sections were cut with a sliding microtome (Microm HM 400) and free floating sections were incubated in 10% normal goat serum followed by incubation in primary antibodies in phosphate buffered saline (PBS) containing triton X-100 (PBS-TX) at the following dilutions: GAP43 (anti-mouse, monoclonal, 1:10,000, Sigma); vesicular GABA transporter (VGAT1, rabbit polyclonal, 1:500, kindly provided by R Reimer); vesicular glutamate transporter (VGLUT1, anti-guinea pig polyclonal, 1:1000, SySy Germany); PSD95 (mouse monoclonal 1:50, NeuroMabs, Davis CA) and NeuN (1:1000, Millipore, Massachusetts USA). Diluted primary antibodies were applied to free floating sections. Incubations were performed for 48 hours on a shaker at 4°C. Sections were then rinsed in PBS and incubated on a shaker at 23°C with species-specific fluorescent secondary antibodies (Molecular Probes, Eugene, Oregon) at a concentration of 1 μg/ml for 2 h. Sections were then mounted on slides using Vectashield Mounting Media (Vector, Burlingame, CA) and stored at 4°C until visualization.

Immunofluorescence was assessed with laser scanning confocal microscopy (Zeiss LSM 510 or Leica SP8). Confocal image stacks were obtained with 0.5 μm separation in the z-axis at 63X and 100X. Image stacks were analyzed in Volocity 2.6.1(Improvision, Perkin Elmer) for volumetric analysis and ImageJ (NIH) for 2-dimensional analysis. The Volocity program allowed the deconvolution of images for visualization and quantification of colocalization of VGLUT1 and PSD95 in close apposition to the somata of biocytin-filled Pyr cells. In later experiments with perfusion-fixed rats, NeuN was used to identify Pyr somata and their boundaries, and tissue processed for PSD95-IR and VGLUT1-IR.

“Train track” analysis: For volumetric analysis of perisomatic objects, Pyr cells were first identified in confocal image stacks as neurons with triangular shaped somata and an apical dendrite projecting towards the pial surface. Cells whose apical dendrite could not be identified were not included in the analyses. The image stack was scanned and cropped in the z-dimension to encompass 4 – 5 sequential 0.5 μm optical sections through the approximate center of the Pyr cell somata. In initial experiments VGAT1 immunoreactivity was used as a guide to demarcate the perisomatic region, as it associates closely with the somata of Pyr neurons (e.g. Fig. 1C; Chaudhry et al., 1998). The inner boundary of the region of interest (ROI) was drawn at the junction of positive perisomatic immunostaining for VGAT1 and the void representing the cell body. The outer boundary was drawn to

Author Manuscript Author Manuscript Author Manuscript Author Manuscript

include immunoreactive VGAT1 puncta in close apposition to the soma. This resulted in a ~3–5 μm wide “train track” around the perisomatic region that extended ~2 μm in the z-dimension. Within the ROI, object identification was restricted by voxel intensity (fluorescence intensity 2 standard deviations from the mean) and size (> 0.2 μm^3). The cumulative volume of the identified objects, i.e. the cumulative volume of the perisomatic protein of interest within the ROI, was expressed as a percentage of the total volume of the ROI. A similar “train track” analysis was used in biocytin-filled neurons and in control and undercut perfusion-fixed rats where somata were identified with NeuN-IR and somatic boundaries could be more accurately delineated.

Biocytin filled cells: We analyzed 5 biocytin-filled layer V Pyr cells from naïve control slices and 7 comparable Pyr cells from undercut cortex. Slices (300 μm) containing labeled neurons were fixed in 4% paraformaldehyde in 0.1 M phosphate buffer overnight at 4°C and reacted for biocytin with fluorescein avidin D (Vector Laboratories, Burlingame, CA). Free-floating slices containing the biocytin-filled cells were labeled with PSD95 plus VGLUT1 using the protocol described above. Images of these slices were collected with the Leica TCS laser scanning SP8 X confocal microscope. Whole biocytin-filled cells, processed with VGLUT1 and PSD95, were imaged with a 40x oil objective. The Volocity program was used to quantitatively analyze z stacks and co-localization. To control for antibody penetration we first determined that all filled cell somata were at comparable depths, close to the surface of the fixed slice. The “find object measurement“ option of Volocity was used to identify the ROI of the filled cell in channel 1 and the colocalized voxels of VGLUT1 and PSD95 in channels 2 and 3 respectively. To measure the volume and intensity of the three channels we used the option of “Standard Deviation 1” for all channels. The intersection of the 3 channels was used to determine colocalization of VGLUT1- and PSD95-IR on somata. Each image stack was rendered into a 3D image using Volocity. For this analysis the inner boundary of the ROI was the edge of the filled pyramidal cell (Fig. 2 C,D) and an outer boundary was selected 2μm outside the inner boundary extending 2μm in the z-axis,. The perisomatic ROI for filled cells was smaller than that for non-filled Pyr cells in which VGAT1 was used to establish somatic margins (above) because the edge of the filled neurons could be more accurately established. Co-localized voxels of VGLUT1/PSD95 that were closely apposed to the soma or dendrites were identified on 7 UC and 5 control filled cells and a “train track” analysis done as above. To further assess the position of VGLUT1/PSD95 voxels on filled cells, 3D movies were made from the Volocity data and cells rotated in the y and x axes. (Supplemental Fig. 1).

Data Analysis

Data compilation, analysis, and presentation were performed with Origin 7 (Origin Labs), Prism 5 (Graphpad) and/or Matlab (Mathworks). All data are expressed as mean ± SEM, unless otherwise noted. Statistical significance between 2 groups was tested by unpaired Student’s t-test or nonparametric Mann-Whitney U test. Significance of difference of cumulative distributions was determined by Kolmogorov-Smirnov (KS) test.

Author Manuscript Author Manuscript Author Manuscript Author Manuscript

RESULTS

Pyramidal cell somata are innervated by new excitatory terminals after injury

We initially used several anatomical approaches to assess potential alterations in excitatory connectivity following partial cortical isolations. GAP-43 is a protein expressed in growth cones and presynaptic terminals during development (Meiri et al., 1986; Goslin et al., 1988; Benowitz and Routtenberg, 1997) and in regenerating axons following damage (McKinney et al., 1997; Yamamoto et al., 2000). Three days after UC, immunoreactivity (IR) for GAP-43 was present within the isolated (UC) cortex and in ipsilateral cortical and subcortical regions, but not in the contralateral unlesioned cortex (Fig. 1A). A similar pattern of GAP-43-IR was observed in 6/6 pairs of matched ipsilateral and contralateral tissue sections from 6 lesioned animals, but not in 0/4 matched pairs from 4 naïve animals (data not shown). In higher resolution single plane confocal images of layer V cortex from UC animals, GAP-43-IR was observed in both the neuropil and also surrounding presumed Pyr neurons (Fig. 1Bii, Cii,iv). VGLUT1-IR was present diffusely in control sections (Bi), but was more prominent in images from UC cortex (Biii) where it was co-localized with GAP-43 in perisomatic halos (Fig. 1Biv, Civ, arrows). This pattern was seen in 30 presumed Pyr cells from 9 confocal sections from 4 UC animals, but not in images from control cortex that were processed in parallel with the UC cortex, using the same immunocytochemical techniques.

To further characterize Pyr cells with perisomatic VGLUT 1 expression, we initially used the immunoreactivity for VGAT1 as a guide to indicate the perisomatic region of Pyr neurons (Fig.1 Di) (Chaudhry et al., 1998; Spruston, 2008). Dual IR for VGLUT1 and VGAT showed that there were VGLUT1-IR puncta close to the presumed somatic margin of Pyr neurons in sections from UC cortex (Fig.1 Dii, arrows). A region of interest (ROI) circumscribing the perisomatic region of layer V Pyr neurons was defined in both lesioned cortex and contralateral homotopic tissue. Volumetric analysis was then performed within an ROI that extended 2μm from the somatic boundary and 1.5μm in the z-axis (Methods). In the contralateral homotopic cortex, 1.82 ± 0.6% of the sampled perisomatic volume of layer V Pyr cells contained VGLUT1 positive voxels, but in the UC cortex, VGLUT1-expressing voxels accounted for 8.52 ± 1.4% of the measured perisomatic volume (14 cells/ROIs analyzed from 9 z-stacks of UC cortex from 3 animals; 6 cells/ROIs analyzed from 3 z-stacks of contralateral cortex from 2 animals; $P < 0.01$, Student's t-test). Together, the data indicate that excitatory axonal terminals form soon after injury and some may aberrantly target the somata of layer V Pyr cells.

Although results of this analysis of Pyr neurons in dual-labeled sections were compatible with the presence of excitatory synapses on somata, the apparent localization of the VGLUT1-IR within the perisomatic ROI might have been due to axonal terminals ending on dendrites of adjacent neurons that passed close to the Pyr somata. To assess VGLUT1-containing terminals in close apposition to PSD95 (putative excitatory synapses) on Pyr somata, we used three other approaches. First, whole cell patch clamp techniques were used to identify layer V Pyr neurons at comparable depths in control and UC slices and fill them with biocytin (Fig. 2A–D). Five filled cells from naïve control slices and 7 comparable Pyr

Author Manuscript Author Manuscript Author Manuscript Author Manuscript

cells from UC cortex were triple-labeled for biocytin, VGLUT1, and PSD95. The Volocity program was used to exclude colocalizations of VGLUT1 and PSD95 that were not in contact with the biocytin-filled cell. In control and UC biocytin-filled cells, VGLUT1- and PSD95-IR close appositions were seen at sites of putative excitatory synapses on dendrites (white arrowheads in Fig. 2A, B; Supplemental Fig. S1). In filled Pyr neurons from UC slices, VGLUT1- and PSD95-IR close appositions were also seen over somata (Fig. 2B, open arrowhead). Close appositions (putative excitatory synapses) at these somatic locations (Fig. 2D, arrows 1–3; D1, D2) as well as on dendrites (arrow 4 in Fig. 2D) were identified in 1 μm images obtained by collapsing two 0.5 μm confocal sections. Single 1 μm optical images cut through somata of the 5 control cells showed VGLUT1- and PSD95-IR and VGLUT1/PSD95 close appositions in the neuropil, but none on somata. Interestingly, some of the PSD95-IR in images from slices that had been maintained in vitro for biocytin cell filling appeared as clusters, as well as puncta (PSD-IR in Fig. 2 C,D). Images from sections of both control and UC biocytin-filled cells contained these PSD95 clusters, although only imaged cells from UC rats had PSD95/VGAT1-IR closely apposed to somata (Table 1). The possibility that injury induced by slicing and incubation of in vitro slices may in some way have altered the expression of PSD95-IR (Gray et al., 2006; Li et al., 2012a) and induced artifactual colocalizations, led us to compare results of Volocity analyses of VGLUT1/PSD95 colocalizations on somata in biocytin-filled cells in immersion-fixed slices with those in tissue from perfusion-fixed rats, where somata were identified with NeuN (Fig. 2E). The sections from perfusion-fixed UC rats also showed close appositions of VGLUT1/PSD95-IR adjacent to somata (Fig. 2E, arrows, 2E1; Fig. 3, S2).

Volumetric analysis with Volocity in the biocytin-filled cells was used to determine the volume of voxels of VGLUT1 that were touching those of PSD95 (presumptive excitatory synapses) and in contact with somata within the ROI (Methods). The Volocity program was set to detect only volumes of particles that fell between 0.5–0.9 μm^3 for PSD95-IR and 0.8–1.3 μm^3 for VGLUT1-IR, and to reject particles outside these ranges. Results from the 7 biocytin-filled neurons from UC cortex (Table 1) showed that 2.87 ± 0.10 % of the perisomatic ROI per cell was occupied by colocalized VGLUT1/PSD95-IR in close apposition to somata. The mean total colocalized volume of VGLUT1/PSD95 within the perisomatic ROI was 7.56 ± 0.49 μm^3 per UC cell (n=7; Table 1) and the combined colocalized VGLUT1/PSD95 particles had volumes in the range of ~1.3–2.2 μm^3. Assuming a colocalized VGLUT1/PSD95 volume of ~1.8 μm^3/neuron, and a total mean colocalized VGLUT1/PSD95 volume of 7.56 μm^3 within the perisomatic ROI/neuron, ~4 synapses would be expected on somata of layer V Pyr neurons in the UC. No colocalization of VGLUT1/PSD95 was found in the perisomatic ROI of the 5 control filled cells (Table 1). The same volumetric analysis was done on 10 cells in 10 sections from each of 2 perfusion-fixed undercut rats and 2 control rats (total 20 UC and 20 control layer V Pyr cells). Volocity detected 2–3 close appositions of VGLUT1/PSD95 puncta on each of the 20 NeuN-labeled somata from UC rats (Fig. 2E, E1). The train track analysis showed that 2.8 ± 0.02% (range 2.2–3.4%) of the ROI volume was occupied by VGLUT1/PSD95-IR close appositions in contact with somata in the 20 UC cells, a value similar to that obtained from biocytin-filled cells (Table 1). In contrast, only 1 VGLUT1/PSD95 close apposition was seen in contact with 1 soma in confocal sections from the 20 control cells. To verify the counts of putative

Author Manuscript Author Manuscript Author Manuscript Author Manuscript

somatic excitatory synapses derived indirectly from the Volocity data, the close appositions of VGLUT1 and PSD95 touching NeuN labeled somata were visually-identified and counted on 10 layer V Pyr cells in each of 3 control and 3 UC rats. Examples of a control and UC cell are shown in Fig. 3. In addition to putative synapses in the neuropil, there were 2–5 (2.97 ± 0.16) putative synapses on somata of all 30 cells from the 3 UC rats (4 white circles adjacent to lower soma in Fig. 3A) and only 1 putative synapse on each of 2 control cells (Fig. 3B, arrow; Table 2 with Graph). Results from visual counts of putative synapses from the perfusion-fixed rats were thus compatible with those from the biocytin-filled neurons (Table 1) and the Volocity data on perfusion-fixed rats (above).

The quantitative data from biocytin-filled cells, or cells from perfused rats, differed from those of presumed Pyr cells in sections from perfused rats where VGAT-IR was used to establish a ROI, and VGLUT1 alone was used as a marker to identify possible somatic excitatory synapses (above). In the later case, uncertainty in estimating the edges of unlabeled Pyr somata led to the use of a larger ROI volume in both the UC and control images. This may have resulted in inclusion of VGLUT1 puncta from axons of adjacent cells in the ROI and the larger volume of VGLUT1 voxels in the ROI of both UC and control cells. To test this possibility we constructed 3-dimensional movies of the filled control and UC Pyr cells from the confocal image stacks (Methods) and rotated the cells in the y and x axes to identify voxels of VGLUT1 and PSD95 that were closely apposed to the soma and dendrites (Fig 2 A,B; Fig. S1). Some PSD95/VGLUT1 profiles that were superimposed on somata became separated from the filled cell during 15° rotation steps and were presumably from closely adjacent dendrites (Fig. S1B, black elipses). However, in 5 rotated UC Pyr cells some PSD95/VGLUT1-IR remained localized over the somata during rotation (Fig. S1A, red elipses). These results are consistent with those obtained in confocal sections through the center of somata (Fig.2C–E; Fig.3; Tables 1 and 2). Taken together, the immunocytochemical data strongly supported the presence of aberrant excitatory synapses on layer V Pyr somata in injured cortex 3 days after the UC cortical injury. We next used electrophysiological approaches to assess potential functional consequences of the anatomical results.

Cortical slices are hyperexcitable 3 days after injury—Whole cell voltage clamp recordings (V_h = −65 mV E_{Cl}^-) were obtained from layer V Pyr cells in acute cortical slices to determine the functional correlates of new excitatory synapse formation after neocortical lesions. From these recordings, spontaneous epileptiform discharges were routinely observed 3 days after UC, but not in control slices. The epileptiform activity was characterized by prolonged (400–1200 ms) bursts of high frequency polysynaptic currents with large amplitudes that often exceeded 1 nA (Salin et al., 1995; Prince and Jacobs, 1998) (Fig.4B, B1). Importantly, the spontaneous epileptiform bursts occurred in normal ACSF without manipulations to increase excitability (i.e. without high potassium, low Mg^{2+}, GABA receptor antagonists, etc.). At least one spontaneous epileptiform discharge was observed in 15/23 brain slices (~65%) from 8/13 UC animals (~62%), but none were recorded in control animals (0/29 slices, 14 animals). Quantification of the epileptiform activity in slices with burst activity showed that bursts occurred with a frequency of 0.4 ± 0.1 bursts per minute and each burst contained EPSCs with a cumulative amplitude of 4.7

Author Manuscript Author Manuscript Author Manuscript Author Manuscript

± 1.8 nA. All-or-none epileptiform discharges with variable latencies were also evoked with extracellular stimulation on column at the deep layer VI-white matter junction and extracellular field potential recordings in layers V and II/III also showed spontaneous epileptiform burst activity (data not shown; see Prince and Tseng, 1993; Hoffman et al, 1994). Because increased excitatory innervation of layer V Pyr neurons after UC could result in hyperexcitable networks that give rise to epileptiform activity (Li and Prince, 2002; Jin et al., 2006; Nicholson et al., 2006; Spruston, 2008), we turned our attention to the frequency and kinetics of EPSCs after injury.

Spontaneous and miniature EPSC frequency is increased after neocortical lesions—To determine if changes in GAP-43 IR and spontaneous epileptiform activity correlated with increases in excitatory synaptic inputs onto layer V Pyr neurons in the UC cortex, we quantified the frequency of spontaneous (s) and miniature (m) EPSCs. Consistent with the observation of increased GAP-43 IR 3 days after UC, the overall frequency of sEPSCs was significantly increased in layer V Pyr cells from UC slices at this time point (2.9 ± 0.4 Hz vs. 5.5 ± 0.8 Hz; control vs. UC slices, respectively; $P < 0.01$). To determine potential changes at the level of individual synapses, mEPSCs were recorded in the presence of 1 μM TTX. mEPSCs occurred with a significantly higher frequency 3 days after UC (2.5 ± 1 Hz vs. 6.6 ± 1.2 Hz; control vs. UC slices, respectively; $P < 0.05$). Assuming no significant differences in the probability of release at excitatory terminals between the 2 groups (however, see Li et al., 2005), the results suggest that layer V Pyr neurons are innervated by more functional excitatory synapses soon after neocortical lesions. These results are similar to those obtained 2–6 weeks after UC lesions in earlier experiments (Li and Prince, 2002), suggesting that an increased excitatory input is maintained over time following the UC.

sEPSC kinetics reflect a redistribution of excitatory synapses—Examples of sEPSCs recorded from control and UC Pyr neurons are shown in Fig. 4. In recordings from injured slices, we often noticed single EPSCs with fast kinetics and large amplitudes (see Fig. 4B, 4B2). Perisomatic or proximal dendritic inputs are hypothesized to evoke currents with faster rise times, larger amplitudes, and narrower half-widths, compared to more distal dendritic inputs, because they are less influenced by electrotonic filtering and space-clamp errors (Spruston et al., 1993; Ulrich and Luscher, 1993; Bekkers and Stevens, 1996; Otmakhova et al., 2002; Williams and Mitchell, 2008). The average amplitudes and kinetics of sEPSCs from control ($n = 29$) and UC ($n = 23$) slices were quantified and are shown in Table 3. The average amplitude of sEPSCs was significantly larger in UC cells (24.9 ± 1.2 pA vs. 38.2 ± 6.5 pA, control vs. UC, respectively; $P < 0.02$) and the 10–90% rise time was also significantly faster (1.89 ± 0.08 ms vs. 1.39 ± 0.07 ms, control vs. UC, respectively; $P < 0.0001$). The average half-width was also significantly shorter in UC slices (5.84 ± 0.32 ms vs. 4.19 ± 0.28 ms, control vs. UC, respectively; $P < 0.001$). However, there was no significant difference in the average charge of sEPSCs (152.3 ± 10.7 fC vs. 185.6 ± 42.8 fC, control vs. UC, respectively $P > 0.5$), likely due to concomitant increases in amplitude and decreases in half-width. Cumulative distributions (Fig. 5A) also showed that 3 days after UC, sEPSCs had larger amplitudes ($d = 0.17$; $P < 0.0001$, KS-test), faster 10–90% rise times

Author Manuscript Author Manuscript Author Manuscript Author Manuscript

(d = 0.25, P < 0.0001, KS-test), and narrower half widths (d = 0.29, P < 0.0001, KS-test), consistent with the averaged data.

Cumulative probabilities and means, however, can mask important details in the distribution of data. In Fig. 5B, the 10–90% rise time of each sEPSC (from the same data set used in 4A) is plotted against its amplitude. The amplitudes of sEPSCs from control cells were all less than 200 pA, with most less than 50 pA (Fig. 4B, left). In UC slices, however, a population of extremely large and fast sEPSCs was clearly evident (events in large blue oval, Fig. 5B, right). These large amplitude sEPSCs ranged from ~100 pA to near 400 pA, with very fast rise times (< 1 ms). There was also a population of sEPSCs with smaller amplitudes and very fast rise times in the UC group (small circle in Fig. 5B, right) that was not present in controls. The majority of the data points in the scatter plots, however, overlapped and appeared similar between groups. Therefore, a cloud density analysis was used to visualize the relative densities within massively overlapping scatter data. The cloud density analysis (the heat maps below the scatter data in Fig. 5B) for sEPSCs from control slices revealed a wide distribution of rise times with the majority ranging from 0.5 to 2.5 ms with a peak in the density map occurring at 1.8 ms (Fig. 5B, left: represented by the region contained within the red contours in the heat map, peak density shown by white dot and crosshairs). However, the same analysis performed on data obtained from UC slices showed a leftward shift in the density of events towards larger amplitudes and faster rise times, the majority of which spanned from 0.5 ms to 1.5 ms with a peak density value occurring at 0.9 ms (Fig. 5B, right: region contained within red contours, peak density shown by white dot and crosshairs). The shift in the density maps from UC recordings is consistent with the faster rise times and larger amplitudes observed in the cumulative distributions and means. The average rise time of sEPSCs from each cell was also plotted against its measured access or input resistance (Fig. 5C). In both groups, faster rise times did not correlate with lower access resistance or higher input resistance, suggesting that differences in neither recording condition nor passive properties contributed to the faster kinetics of sEPSCs from the UC group.

To determine if differences at the level of individual synapses underlie the faster and larger sEPSCs, the kinetics and amplitudes of mEPSCs in the presence of TTX from control (n = 11 cells) and UC (n = 10 cells) slices were also analyzed and the results are summarized in Table 4. In contrast to sEPSCs, there were no statistical differences in the mean amplitude, rise time, or half width of averaged mEPSCs between control and UC slices. However, cumulative distributions made from 50 randomly selected events from each cell showed a small but statistically significant difference in the amplitude (d = 0.13, P < 0.001), but not in the half width or 10–90% rise time of mEPSCs from UC slices (Fig. 6A). A scatter plot of the data showed a small population of mEPSCs in the UC group with fast rise times that was not present in controls (see shaded boxes in Fig. 6B), however an overall shift towards faster rise times or larger amplitudes was not observed in the cloud density analysis (Fig. 6B, heat maps). The results suggest that release probabilities and kinetics on a per synapse basis are not significantly different between UC and control slices and argue for action potential-dependent activation of more proximal inputs as a potential mechanism underlying the larger amplitudes and faster rise times of sEPSCs recorded in UC slices. The data also suggest a population of mEPSCs that have the characteristics of proximal inputs (larger amplitudes,

Author Manuscript Author Manuscript Author Manuscript Author Manuscript

faster rise times), but due to their infrequency, probably did not contribute to an overall difference in the data.

Apparent EPSC reversal potentials reflect electrotonically proximal synapses in lesioned neocortex—The above analysis supports the hypothesis that a population of excitatory inputs onto Pyr cells is more proximately located in the lesioned cortex than in control cortex. Due to technical difficulties in space clamping distal membranes (i.e. electrotonic filtering), proximal synaptic currents should also appear to have negatively shifted reversal potentials compared to currents generated from electrotonically distant inputs (Carnevale and Johnston, 1982; Spruston et al., 1993; Otmakhova et al., 2002; Smeal et al., 2008). To further investigate this possibility, we focally stimulated afferents in the perisomatic region by placing a small tip diameter theta glass electrode within 20 μm of the soma of the recorded cell (Fig. 7A).

Stimulus amplitude was fixed for each experiment, but in order to standardize the stimulation parameters, the duration was adjusted for each cell in step-wise fashion until the first evoked response above threshold was reliably detected. To calculate AMPA-mediated reversal potentials, NMDA and $GABA_A$ receptors were blocked, Pyr neurons were voltage clamped, and an EPSC was evoked with focal stimulation at various negative and positive holding potentials (Fig. 7B). The normalized peak amplitude for an averaged EPSC at each holding potential was plotted and a linear regression line was fit for each cell (Fig. 7C). The evoked amplitudes at each V_h from −20 to +40 mV were significantly different between UC and control slices (Fig. 7C) and the average AMPA-mediated reversal potential from UC slices was significantly negatively shifted compared to reversal potentials in control slices (control: 25.5 ± 4.4 mV, n = 10 cells; UC: 10.5 ± 4 mV, n = 8 cells, $P < 0.05$). These results suggest that focal stimulation near layer V Pyr cells in UC slices activated excitatory inputs that terminated closer to the soma, as compared to those evoked by afferent stimulation in control slices.

Laser scanning photostimulation (LSPS) evokes large amplitude EPSCs in slices from UC neocortex—Functional connections in a neuronal circuit can be mapped by recording LSPS-evoked post-synaptic currents from a single neuron while depolarizing neighboring neurons to threshold by focal glutamate uncaging (Shepherd et al., 2003; Deleuze and Huguenard, 2006; Jin et al., 2006, 2011). We recorded layer V Pyr neurons from slices of control (n = 14 cells from 5 animals) and UC (n = 17 cells from 8 animals) animals and used LSPS to activate functionally connected presynaptic neurons to determine the laminar locations of putative excitatory neurons that may have formed perisomatic terminals. Figure 8A–C shows an example data set from an UC slice containing several large amplitude LSPS-evoked EPSCs. For this particular experiment, stimulus locations spanned the cortical layers and each location was separated by 75 μm (Fig. 8A inset). A 200 μs “flash” from a pulsed UV laser was used to uncage glutamate at each location while recording from a voltage clamped layer V Pyr neuron (cell location indicated by red circle, inset). The recorded currents in response to laser uncaging at each location are shown in Fig. 8A. The evoked events were sorted as either direct responses from glutamate uncaged directly on the recorded neuron (black “+”) or putative monosynaptic EPSCs (red circles at

Author Manuscript Author Manuscript Author Manuscript Author Manuscript

peaks) based on onset latency. The peak amplitudes of putative monosynaptic EPSCs were displayed as a heat map (Fig. 8B), which shows the amplitudes of the EPSC, the location of the recorded neuron (white circle), and the location(s) of putative presynaptic cell(s) making functional connections with the recorded neuron (direct responses are omitted from the heat map). The arrow in Fig. 8B points to one “hot spot” in which a single-peak large amplitude EPSC was evoked by glutamate uncaging. This particular EPSC could be repeatedly evoked by uncaging glutamate at the same location and its occurrence appeared to be “all-or-none” (Fig. 8C). The properties of this evoked current, including absence of any inflections on its rising phase and unchanging latency and amplitude when the stimulus intensity was doubled (Fig. 8C), suggested that it may have resulted from activation of a connected pair of neurons. Similar all-or-none EPSCs were recorded in 4 neurons where the stimulus intensity (laser duration) was varied. A representative map constructed from evoked EPSCs across 5 trials from a different cell in an UC slice is shown in Fig. 8D. At several stimulus locations, large amplitude single peak EPSCs > 100 pA were repeatedly evoked. Two representative maps from control slices are shown in Figure 8E. The peak amplitudes of evoked EPSCs in the control maps shown are all under 100 pA in amplitude and, therefore, smaller than those in the UC maps of 7B and 7D.

Large amplitude EPSCs were typically not evoked in control maps. A single laser--evoked EPSC >100 pA was evoked in only 1 of 14 control slices from a total of 3850 laser photostimulus sites, or ~.026 % of sampled locations, and this response was evoked from only from a single location in that slice. In contrast, large amplitude EPSCs were evoked in 5 out of 17 slices from UC animals. On average, UC maps showing large amplitude events had 4.2 ± 1.6 locations from which such events could be triggered. A total of 21 large amplitude EPSCs was evoked from 4675 LSPS locations in 17 UC maps, or ~0.45% of stimulated sites in undercut cortex, The difference in the fraction of locations that evoked large amplitude EPSCs (i.e. total number of large amplitude EPSCs / total number of locations sampled) was statistically different between control and UC slices ($P<0.001$, Chi-square test)

To visualize the distribution of large amplitude EPSCs, maps were registered to one another based on laminar orientation and location of the recorded neuron, and large amplitude hot spots were summed across maps (Fig. 8F). This analysis of both laminar and columnar dimensions showed that the large amplitude events could be evoked by stimulating presynaptic cells in multiple layers, both within a single column and also from adjacent columns. In general, large amplitude EPSCs were evoked in UC slices from layer V and layers both deep and superficial to the recorded neuron and from cortical columns within and adjacent to the recording site. The maps in Fig. 8F (right) suggest that local rewiring originating from these locations may contribute to the generation of large amplitude EPSCs after injury. Comparison of the number of maps with large amplitude events from UC animals (5 of 17 mapping experiments from 8 UC animals) to control animals (1 of 14 experiments from 5 control animals) showed a statistically significant difference ($P < 0.01$, Chi-square test). Cumulative distributions of the peak amplitudes of evoked EPSCs also showed a statistically significant shift for large amplitude EPSCs in slices from UC animals (Fig.8G, $n = 348$ vs. $n = 273$ evoked events in control and UC, respectively, $P < 0.05$), consistent with the cumulative distributions of sEPSC amplitudes (Fig. 5A).

Author Manuscript Author Manuscript Author Manuscript Author Manuscript

Discussion

Alterations in neuronal circuits after injury

In this study, immunostaining for GAP-43, a protein found in growth cones and sprouting axons during development and regeneration following damage (Meiri et al., 1986; Goslin et al., 1988; Benowitz and Routtenberg, 1997; McKinney et al., 1997; Yamamoto et al., 2000), was increased in and around the UC cortex 3 days after a lesion. In other studies, excitatory neurons have been shown to sprout new axons within several days after fluid percussion injury (Povlishock and Kontos, 1985), following lesions to the axonal tract of corticospinal projecting neurons (Fishman and Mattu, 1993), after diffuse axonal injury (Greer et al., 2011), and cortical stab wounds (King et al., 2001). Furthermore, transection of Schaffer collaterals up-regulates GAP-43 within 3 days, concurrent with formation of recurrent excitatory connections and a hyperexcitable hippocampal network (McKinney et al., 1997). Our results are consistent with the conclusion that excitatory axons in cortex can sprout and form functional connections soon after injury. We previously studied axons of layer V Pyr cells in the UC cortex 36–84 days after the UC lesion and found significant sprouting, evidenced by increases of ~65% in axonal collaterals and ~115% in synaptic boutons, especially prominent in layer V (Salin et al, 1995). The present results show that this axonal reorganization begins at least as early as 3 days after injury and is associated with functional alterations in excitatory neocortical networks. Further, our results suggest that this acute reorganization in the lesioned cortex may be maladaptive and promote network hyperexcitability and epileptiform activity in the UC cortex. Earlier experiments in the UC model showed that these functional network alterations can persist for weeks after the UC (Prince and Tseng, 1993; Jin et al., 2006),

The targeting of new excitatory axon collaterals to the somata of layer V Pyr cells, suggested by the immunocytochemical data of Figs. 1B, 2, 3, S1, and Tables 1–2, is a novel finding of these experiments. Excitatory terminals usually synapse on spines and shafts of Pyr cell dendrites while the somata are innervated primarily by inputs from inhibitory cells (Levay, 1973; Parnavelas et al., 1977; Mcguire et al., 1991; reviewed in Salin and Bullier, 1995 and Spruston, 2008). Perisomatic excitatory synapses would hypothetically depolarize the somatic membrane potential to a larger extent than distal inputs, and therefore increase neuronal excitability (Schubert et al., 2001; Williams and Stuart, 2002, 2003; Nicholson et al., 2006; Spruston, 2008). The results of our immunocytochemical experiments support the presence of glutamatergic synapses on layer V Pyr somata within 3 days of the UC injury. The kinetics of sEPSCs recorded from layer V Pyr neurons in UC cortex were faster and amplitudes larger, consistent with the anatomical results that suggested an increase in perisomatic excitatory terminals (Fig. 5). However, although cumulative plots of mEPSC also showed increases in amplitude, there were no significant decreases in rise time or half width (Fig. 6). One possible explanation for this difference would be presynaptic alterations in newly-formed immature synapses affecting release machinery. For example, alterations in BDNF expression, known to be present in undercut cortex (Prince et al, 2009), can affect EPSC parameters in neocortex and thalamus through actions at presynaptic sites (Taniguchi et al., 2000; Laudes et al., 2012) .

Author Manuscript Author Manuscript Author Manuscript Author Manuscript

Further support for aberrant proximal excitatory inputs is provided by the negatively shifted reversal potential of AMPA receptor-mediated EPSCs evoked by focal perisomatic stimulation of layer V afferents in the injured cortex. This apparent shift in EPSC reversal potential would be expected because proximal synapses would be less affected by electrotonic filtering and space clamp errors (Spruston et al., 1993; Otmakhova et al., 2002; Smeal et al., 2008; Williams and Mitchell, 2008). The potential contribution of increased excitatory somatic innervation to network hyperexcitability is difficult to estimate without data on the density of the aberrant somatic innervation, the functional properties of these synapses and parallel alterations that may occur in dendritic structure and function.

Laser scanning photostimulation of caged glutamate was used to directly depolarize presynaptic neurons and map excitatory synaptic connectivity. Results are compatible with those from analyses of sEPSCs; large amplitude laser uncaging-evoked EPSCs were more frequent in injured slices than in controls. However, rise times for uncaging-evoked EPSCs were not shifted towards faster events, in contrast to those in the recordings of sEPSCs. This may be accounted for by differences in temperature in the two sets of experiments, i.e. ~23°C in LSPS experiments (Jin et al, 2006) and more physiological temperatures (32°C) for sEPSCs. Slower kinetics of synaptic potentials and action potentials at cooler temperatures (Thompson et al, 1985), as well as slower rates of glutamate transport (Bergles and Jahr, 1998), might have obscured differences in EPSC kinetics between control and UC in LSPS experiments.

A number of different mechanisms, aside from proximal inputs, could underlie the large amplitude sEPSCs and uncaging-evoked EPSCs. Increased number of synapses from a Pyr cell onto a given target Pyr neuron, an increased probability of release (P_r), or an increased density of post synaptic receptors could influence the magnitude of recorded synaptic currents. Several weeks after UC, layer V Pyr neurons show a significant increase in paired-pulse depression, which may indicate an increased P_r of glutamate from excitatory terminals (Li et al, 2005); however, P_r at this synapse has not been investigated early after UC. The mEPSC amplitudes in the current study were significantly larger (by KS-test), which might result from a post-synaptic modification in the density of postsynaptic receptors, multivesicular release (Christie and Jahr, 2006), or increased glutamate content in single vesicles (Erickson et al., 2006).

The large amplitude uncaging-evoked EPSCs and the population of large and fast sEPSCs are also interesting, considering that the peak amplitudes of unitary EPSCs between layer V Pyr cells in frontal cortex range from ~15 to 18 pA (Morishima and Kawaguchi, 2006). Markram et al. (1997) recorded unitary EPSPs between layer V Pyr cells in somatosensory cortex that ranged from 0.15 to 5.5 mV, which by our calculations correspond to unitary EPSCs ranging from ~1.5 to 55 pA (assuming that R_m = 100 MΩ). Therefore, to evoke a ~200 pA EPSC, synchronous activation of roughly 4 to 15 connections would be required, assuming that multivesicular release was not present. The absence of inflections on the rising phase of uncaging-evoked EPSCs in Fig. 8C and on the large amplitude spontaneous EPSCs (example in Fig. 4B2) suggests that the axon from a single neuron in the injured cortex may make multiple synaptic contacts onto any given neighboring postsynaptic neuron such that a single action potential results in the nearly simultaneous activation of multiple

Author Manuscript Author Manuscript Author Manuscript Author Manuscript

excitatory inputs that sum to produce a single evoked EPSC > 100 pA. This result would be in contrast to studies in injured hippocampus (McKinney et al., 1997) and chronic UC neocortex (Jin et al. 2006) that suggest a lack of hyper-innervation to single targets from sprouting Pyr neurons. Additional anatomical analysis of single filled Pyr cells and their postsynaptic targets would be required to clarify this point.

Spontaneous epileptiform activity after injury

Robust spontaneous epileptiform activity in UC slices was present in recordings from layer V Pyr neurons. We confirmed that these events were network-related with extracellular recordings and by evoking burst activity with electrical stimulation. We hypothesize that increased recurrent excitatory connectivity early after injury contributes to the observed cortical hyperexcitability. Such hyperexcitability can occur in vivo within minutes to days after controlled cortical impact injury (Nilsson et al., 1994; Yang et al., 2010). In the UCs of ketamine/xylazine-anesthetized, but not barbiturate-anesthetized cats, hyperexcitability and epileptiform EEG activity is present within a few hours after white matter lesions (Topolnik et al., 2003a, 2003b). Mechanisms for early hyperexcitability could include enhanced excitatory inputs to layer V Pyr cells (Yang and Benardo, 1997; Yang et al., 2007), alterations in intrinsic properties (Topolnik et al., 2003a, 2003b), and increases in extracellular potassium and glutamate (D'Ambrosio et al., 1999; David et al., 2009). Disruption to the blood brain barrier (Seiffert et al., 2004; Ivens et al., 2007; Cacheaux et al., 2009) and inflammatory cytokines (Vezzani et al., 2000, 2008; Vezzani and Granata, 2005; Ravizza et al., 2008) released after TBI can also be epileptogenic.

Other pathophysiological abnormalities specific to this model also likely occur in parallel with the alterations described in the current experiments. For example, decreased efficacy of GABAergic transmission (Li and Prince, 2002; Faria and Prince, 2010; Jin et al., 2011; Faria et al., 2012; Ma and Prince, 2012) and changes in membrane properties of the injured Pyr neurons present in chronic UC (Prince and Tseng, 1993) or after axotomy (Tseng and Prince, 1996) might also be present early. There may also be changes in the composition of postsynaptic glutamate receptors early after injury (Kharazia and Prince, 2001). Our results do not rule out a contribution from excitatory synaptic potentiation due to injury or as a result of epileptiform activity *per se*. Some studies do show that epileptiform activity may strengthen excitatory transmission (eg. Kapur and Haberly, 1998; Abegg et al., 2004); however other reports do not support a close link between potentiation (e.g. LTP) and generation of epileptiform events (Leung, 1994). In any case, potentiation alone would not be expected to alter the EPSC reversal potential (e.g. Fig. 7). The large variety of injury-induced changes in this and other models of posttraumatic epileptogenesis makes it difficult to predict the most important contributing pathophysiological event.

Previous work from our laboratory has identified the first 3 days as a critical time window for acquiring chronic neocortical hyperexcitability in vitro following an UC lesion. TTX, a potent blocker of action potential dependent synaptic activity, administered within the first 3 days after UC significantly reduced the occurrence of epileptiform activity in neocortical slices (Graber and Prince, 1999, 2004), perhaps by decreasing activity-dependent axonal spouting (Prince et al., 2009). Similarly, gabapentin, a compound that interferes with

Author Manuscript Author Manuscript Author Manuscript Author Manuscript

synapse formation during development by inhibiting the interaction of astrocyte-secreted thrombospondins with α2δ-1 calcium channel subunit receptors (Eroglu et al., 2009), also reduced neocortical hyperexcitability and *in vitro* epileptogenesis in this model, if applied within the first 3 days (Li et al., 2012b). These results suggest that limiting excitatory synapse formation early after injury could curtail the development of chronic hyperexcitability. Our present results expand on these findings by showing that rapid reorganization of excitatory circuits is accompanied by spontaneous in vitro epileptiform activity 3 days after neocortical lesions. Such increases in excitatory activity, if present in human TBI, could contribute to the occurrence of early seizures that follow severe cortical injury and may play a role in the development of chronic TBI-induced epilepsy.

Supplementary Material

Refer to Web version on PubMed Central for supplementary material.

Acknowledgments

This work was supported by NINDS Grants NS12151, NS39579 and NS82644 to DAP and postdoctoral fellowship (F32) NS077623 to DKT. Daniel Richter provided preliminary anatomical results. We thank John Huguenard for advice in laser scanning and confocal experiments and Paul Buckmaster for helpful suggestions regarding analysis of putative synapses.

Abbreviations

mEPSCs/sEPSCs	miniature and spontaneous excitatory postsynaptic currents
LSPS	laser scanning photostimulation
TBI	traumatic brain injury
GAP43	growth-associated protein-43
VGLUT1	vesicular glutamate transporter1
PSD95	postsynaptic density 95
VGAT	vesicular GABA transporter
UC	undercut, partially isolated neocortex

References

Abegg MH, Savic N, Ehrengruber MU, McKinney RA, Gähwiler BH. Epileptiform activity in rat hippocampus strengthens excitatory synapses. J Physiol. 2004; 554:439–448. [PubMed: 14594985]

Avramescu S, Nita DA, Timofeev I. Neocortical Post-Traumatic Epileptogenesis Is Associated with Loss of GABAergic Neurons. J Neurotrauma. 2009; 26:799–812. Available at: ISI: 000266574500014. [PubMed: 19422294]

Beghi E, Carpio A, Forsgren L, Hesdorffer DC, Malmgren K, Sander JW, Tomson T, Hauser WA. Recommendation for a definition of acute symptomatic seizure. Epilepsia. 2010; 51:671–675. Available at: http://www.ncbi.nlm.nih.gov/pubmed/19732133. [PubMed: 19732133]

Bekkers JM, Stevens CF. Cable properties of cultured hippocampal neurons determined from sucrose-evoked miniature EPSCs. J Neurophysiol. 1996; 75:1250–1255. Available at: ISI:A1996UA06200024. [PubMed: 8867133]

Author Manuscript Author Manuscript Author Manuscript Author Manuscript

Benowitz LI, Routtenberg A. GAP-43: An intrinsic determinant of neuronal development and plasticity. Trends Neurosci. 1997; 20:84–91. Available at: http://www.ncbi.nlm.nih.gov/pubmed/9023877. [PubMed: 9023877]

Bergles DE, Jahr CE. Glial contribution to glutamate uptake at Schaffer collateral-commissural synapses in the hippocampus. J Neurosci. 1998; 18:7709–7716. Available at: http://www.ncbi.nlm.nih.gov/pubmed/9742141. [PubMed: 9742141]

Cacheaux LP, Ivens S, David Y, Lakhter AJ, Bar-Klein G, Shapira M, Heinemann U, Friedman A, Kaufer D. Transcriptome profiling reveals TGF-beta signaling involvement in epileptogenesis. J Neurosci. 2009; 29:8927–8935A. [PubMed: 19605630]

Carmichael ST. Plasticity of cortical projections after stroke. Neuroscientist. 2003; 9:64–75. Available at: ISI:000180642300015. [PubMed: 12580341]

Carnevale NT, Johnston D. Electro-Physiological Characterization of Remote Chemical Synapses. J Neurophysiol. 1982; 47:606–621. Available at: ISI:A1982NK13700005. [PubMed: 7069456]

Chaudhry F, Reimer R, Bellocchio E, Danbolt N, Osen K, Edwards R, Storm-Mathisen J. The vesicular GABA transporter, VGAT, localizes to synaptic vesicles in sets of glycinergic as well as GABAergic neurons. J Neurosci. 1998; 18:9733–9750. Available at: http://www.ncbi.nlm.nih.gov/pubmed/9822734. [PubMed: 9822734]

Christie JM, Jahr CE. Multivesicular release at Schaffer collateral-CA1 hippocampal synapses. J Neurosci. 2006; 26:210–216. Available at: http://www.pubmedcentral.nih.gov/articlerender.fcgi?artid=2670931&tool=pmcentrez&rendertype=abstract. [PubMed: 16399689]

Chuckowree JA, Dickson TC, Vickers JC. Intrinsic regenerative ability of mature CNS neurons. Neuroscientist. 2004; 10:280–285. Available at: http://www.ncbi.nlm.nih.gov/pubmed/15271255. [PubMed: 15271255]

Cohen AS, Pfister BJ, Schwarzbach E, Grady MS, Goforth PB, Satin LS. Injury-induced alterations in CNS electrophysiology. Brain. 2007; 161:143–169.

Cohen, I.; Miles, R. [Accessed November 16, 2012] Contributions of intrinsic and synaptic activities to the generation of neuronal discharges in in vitro hippocampus; J Physiol. 2000. p. 485-502.Available at: http://jp.physoc.org/content/524/2/485.short

D'Ambrosio R, Fairbanks JP, Fender JS, Born DE, Doyle DL, Miller JW. Post-traumatic epilepsy following fluid percussion injury in the rat. Brain. 2004; 127:304–314. Available at: ISI:000188389900007. [PubMed: 14607786]

D'Ambrosio R, Maris DO, Grady MS, Winn HR, Janigro D. Impaired K(+) homeostasis and altered electrophysiological properties of post-traumatic hippocampal glia. J Neurosci. 1999; 19:8152–8162. Available at: ISI:000082539900047. [PubMed: 10479715]

David Y, Cacheaux LP, Ivens S, Lapilover E, Heinemann U, Kaufer D, Friedman A. Astrocytic dysfunction in epileptogenesis: consequence of altered potassium and glutamate homeostasis? J Neurosci. 2009; 29:10588–10599. [PubMed: 19710312]

DeFelipe, J.; Jones, EG. Cajal's Degeneration and Regeneration of the Nervous System. New York: Oxford; 1991. Available at: http://books.google.com/books?id=EpulffDsBOEC

Deleuze C, Huguenard JR. Distinct electrical and chemical connectivity maps in the thalamic reticular nucleus: potential roles in synchronization and sensation. J Neurosci. 2006; 26:8633–8645. Available at: http://www.ncbi.nlm.nih.gov/pubmed/16914689. [PubMed: 16914689]

Erickson JD, De Gois S, Varoqui H, Schafer MK-H, Weihe E. Activity-dependent regulation of vesicular glutamate and GABA transporters: a means to scale quantal size. Neurochem Int. 2006; 48:643–649. Available at: http://www.ncbi.nlm.nih.gov/pubmed/16546297. [PubMed: 16546297]

Eroglu C, Allen NJ, Susman MW, O'Rourke NA, Park CY, Ozkan E, Chakraborty C, Mulinyawe SB, Annis DS, Huberman AD, Green EM, Lawler J, Dolmetsch R, Garcia KC, Smith SJ, Luo ZD, Rosenthal A, Mosher DF, Barres BA. Gabapentin Receptor alpha 2 delta-1 Is a Neuronal Thrombospondin Receptor Responsible for Excitatory CNS Synaptogenesis. Cell. 2009; 139:380–392. Available at: ISI:000270857500020. [PubMed: 19818485]

Faria LC, Parada I, Prince DA. Interneuronal calcium channel abnormalities in posttraumatic epileptogenic neocortex. Neurobiol Dis. 2012; 45:821–828. Available at: http://www.ncbi.nlm.nih.gov/pubmed/22172650. [PubMed: 22172650]

Author Manuscript Author Manuscript Author Manuscript Author Manuscript

Faria LC, Prince DA. Presynaptic Inhibitory Terminals Are Functionally Abnormal in a Rat Model of Posttraumatic Epilepsy. J Neurophysiol. 2010; 104:280–290. Available at: ISI:000279586400026. [PubMed: 20484536]

Fishman PS, Mattu A. Fate of severed cortical projection axons. J Neurotrauma. 1993; 10:457–470. [PubMed: 8145268]

Frey LC. Epidemiology of posttraumatic epilepsy: A critical review. Epilepsia. 2003; 44:11–17. Available at: http://www.ncbi.nlm.nih.gov/pubmed/14511389. [PubMed: 14511389]

Goslin K, Schreyer DJ, Skene JHP, Banker G. Development of Neuronal Polarity - Gap-43 Distinguishes Axonal from Dendritic Growth Cones. Nature. 1988; 336:672–674. Available at: ISI:A1988R363900056. [PubMed: 3059197]

Graber KD, Prince DA. Tetrodotoxin prevents posttraumatic epileptogenesis in rats. Ann Neurol. 1999; 46:234–242. Available at: http://www.ncbi.nlm.nih.gov/pubmed/10443889. [PubMed: 10443889]

Graber KD, Prince DA. A critical period for prevention of posttraumatic neocortical hyperexcitability in rats. Ann Neurol. 2004; 55:860–870. Available at: http://www.ncbi.nlm.nih.gov/pubmed/15174021. [PubMed: 15174021]

Graber, KD.; Prince, DA. Chronic Partial Cortical Isolation. In: Pitkänen, A.; Schwartzkroin, PA.; Moshe, SL., editors. Models of Seizures and Epilepsy. San Diego: Elsevier; 2006. p. 477-493.Available at: http://www.sciencedirect.com/science/article/B8433-4N1SVB4-9/2/cce175ad1961174165f7c844ade7620e

Gray NW, Weimer RM, Bureau I, Svoboda K. Rapid redistribution of synaptic PSD-95 in the neocortex in vivo. PLoS Biol. 2006; 4:2065–2075.

Greer JE, Mcginn MJ, Povlishock JT. Diffuse Traumatic Axonal Injury in the Mouse Induces Atrophy, c-Jun Activation, and Axonal Outgrowth in the Axotomized Neuronal Population. J Neurosci. 2011; 31:5089–5105. Available at: ISI:000288938200034. [PubMed: 21451046]

Hauser WA, Annegers JF, Kurland LT. Prevalence of Epilepsy in Rochester, Minnesota - 1940–1980. Epilepsia. 1991; 32:429–445. Available at: ISI:A1991GD06300001. [PubMed: 1868801]

Herman ST. Epilepsy after brain insult - Targeting epileptogenesis. Neurology. 2002; 59:S21–S26. Available at: http://www.ncbi.nlm.nih.gov/pubmed/12428028. [PubMed: 12428028]

Hoffman SN, Salin PA, Prince DA. Chronic neocortical epileptogenesis in vitro. J Neurophysiol. 1994; 71:1762–1773. Available at: http://www.ncbi.nlm.nih.gov/pubmed/8064347. [PubMed: 8064347]

Ivens S, Kaufer D, Flores LP, Bechmann I, Zumsteg D, Tomkins O, Seiffert E, Heinemann U, Friedman A. TGF-beta receptor-mediated albumin uptake into astrocytes is involved in neocortical epileptogenesis. Brain. 2007; 130:535–547. Available at: http://www.ncbi.nlm.nih.gov/pubmed/17121744. [PubMed: 17121744]

Jin X, Huguenard JR, Prince DA. Reorganization of inhibitory synaptic circuits in rodent chronically injured epileptogenic neocortex. Cereb Cortex. 2011; 21:1094–1104. Available at: http://www.pubmedcentral.nih.gov/articlerender.fcgi?artid=3077430&tool=pmcentrez&rendertype=abstract. [PubMed: 20855494]

Jin X, Prince DA, Huguenard JR. Enhanced excitatory synaptic connectivity in layer V pyramidal neurons of chronically injured epileptogenic neocortex in rats. J Neurosci. 2006; 26:4891–4900. Available at: ISI:000237271700020. [PubMed: 16672663]

Kapur A, Haberly LB. Duration of NMDA-dependent synaptic potentiation in piriform cortex in vivo is increased after epileptiform bursting. J Neurophysiol. 1998; 80:1623–1629. [PubMed: 9772226]

Kharazia VN, Prince DA. Changes of alpha-amino-3-hydroxy-5-methyl-4-isoxazole-propionate receptors in layer V of epileptogenic, chronically isolated rat neocortex. Neuroscience. 2001; 102:23–34. Available at: http://www.ncbi.nlm.nih.gov/pubmed/11226667. [PubMed: 11226667]

King CE, Canty AJ, Vickers JC. Alterations in neurofilaments associated with reactive brain changes and axonal sprouting following acute physical injury to the rat neocortex. Neuropathol Appl Neurobiol. 2001; 27:115–126. Available at: http://doi.wiley.com/10.1046/j.1365-2990.2001.00317.x. [PubMed: 11437992]

Kraus JF, McArthur DL. Epidemiologic aspects of brain injury. Neurol Clin. 1996; 14:435. Available at: ISI:A1996UM72300014. [PubMed: 8827181]

Laudes T, Meis S, Munsch T, Lessmann V. Impaired transmission at corticothalamic excitatory inputs and intrathalamic GABAergic synapses in the ventrobasal thalamus of heterozygous BDNF

Author Manuscript Author Manuscript Author Manuscript Author Manuscript

knockout mice. Neuroscience. 2012; 222:215–227. Available at: http://www.ncbi.nlm.nih.gov/pubmed/22796079. [PubMed: 22796079]

Leung LW. Evaluation of the hypothesis that hippocampal interictal spikes are caused by long-term potentiation. Epilepsia. 1994; 35:785–794. Available at: http://www.ncbi.nlm.nih.gov/pubmed/8082623. [PubMed: 8082623]

Levay S. Synaptic Patterns in Visual-Cortex of Cat and Monkey - Electron-Microscopy of Golgi Preparations. J Comp Neurol. 1973; 150:53–85. Available at: ISI:A1973Q011200003. [PubMed: 4124647]

Li C, Zhou Y, Liu Z, Tuo J, Hu N, Guan H. Spatiotemporal expression of postsynaptic density 95 in rat retina after optic nerve injury. J Mol Neurosci. 2012a; 46:595–605. Available at: http://www.ncbi.nlm.nih.gov/pubmed/21927888. [PubMed: 21927888]

Li H, Bandrowski AE, Prince DA. Cortical Injury Affects Short-Term Plasticity of Evoked Excitatory Synaptic Currents. J Neurophysiol. 2005; 93:146–156. [PubMed: 15342719]

Li H, Graber KD, Jin S, McDonald W, Barres BA, Prince DA. Gabapentin decreases epileptiform discharges in a chronic model of neocortical trauma. Neurobiol Dis. 2012b; 48:429–438. Available at: http://www.ncbi.nlm.nih.gov/pubmed/22766033. [PubMed: 22766033]

Li H, McDonald W, Parada I, Faria L, Graber KD, Takahashi DK, Ma Y, Prince DA. Targets for preventing epilepsy following cortical injury. Neurosci Lett. 2011; 497:172–176. Available at: ISI:000292411600004. [PubMed: 21354270]

Li H, Prince DA. Synaptic activity in chronically injured, epileptogenic sensory-motor neocortex. J Neurophysiol. 2002; 88:2–12. Available at: http://www.ncbi.nlm.nih.gov/pubmed/12091528. [PubMed: 12091528]

Lowenstein DH. Epilepsy after head injury: An overview. Epilepsia. 2009; 50:4–9. Available at: ISI:000262827500002. [PubMed: 19187288]

Ma Y, Prince DA. Functional alterations in GABAergic fast-spiking interneurons in chronically injured epileptogenic neocortex. Neurobiol Dis. 2012; 47:102–113. Available at: http://www.ncbi.nlm.nih.gov/pubmed/22484482. [PubMed: 22484482]

Markram H, Lübke J, Frotscher M, Roth A, Sakmann B. Physiology and anatomy of synaptic connections between thick tufted pyramidal neurones in the developing rat neocortex. J Physiol. 1997; 500:409–440. Available at: http://www.pubmedcentral.nih.gov/articlerender.fcgi?artid=1159394&tool=pmcentrez&rendertype=abstract. [PubMed: 9147328]

Mcguire BA, Gilbert CD, Rivlin PK, Wiesel TN. Targets of Horizontal Connections in Macaque Primary Visual-Cortex. J Comp Neurol. 1991; 305:370–392. Available at: ISI:A1991FB93800002. [PubMed: 1709953]

McKinney RA, Debanne D, Gahwiler BH, Thompson SM, Gähwiler BH. Lesion-induced axonal sprouting and hyperexcitability in the hippocampus in vitro: implications for the genesis of posttraumatic epilepsy. Nat Med. 1997; 3:990–996. Available at: http://www.ncbi.nlm.nih.gov/pubmed/9288725. [PubMed: 9288725]

Meiri KF, Pfenninger KH, Willard MB. Growth-Associated Protein, Gap-43, A Polypeptide That Is Induced When Neurons Extend Axons, Is A Component of Growth Cones and Corresponds to Pp46, A Major Polypeptide of A Subcellular Fraction Enriched in Growth Cones. Proc Natl Acad Sci U S A. 1986; 83:3537–3541. Available at: ISI:A1986C379200104. [PubMed: 3517863]

Morishima M, Kawaguchi Y. Recurrent connection patterns of corticostriatal pyramidal cells in frontal cortex. J Neurosci. 2006; 26:4394–4405. Available at: http://www.ncbi.nlm.nih.gov/pubmed/16624959. [PubMed: 16624959]

Nicholson DA, Trana R, Katz Y, Kath WL, Spruston N, Geinisman Y. Distance-dependent differences in synapse number and AMPA receptor expression in hippocampal CA1 pyramidal neurons. Neuron. 2006; 50:431–442. Available at: http://www.ncbi.nlm.nih.gov/pubmed/16675397. [PubMed: 16675397]

Nilsson P, Ronne-Engström E, Flink R, Ungerstedt U, Carlson H, Hillered L, Ronne-Engstrom E. Epileptic seizure activity in the acute phase following cortical impact trauma in rat. Brain Res. 1994; 637:227–232. Available at: http://www.ncbi.nlm.nih.gov/pubmed/8180800. [PubMed: 8180800]

Author Manuscript Author Manuscript Author Manuscript Author Manuscript

Otmakhova NA, Otmakhov N, Lisman JE. Pathway-specific properties of AMPA and NMDA-mediated transmission in CA1 hippocampal pyramidal cells. J Neurosci. 2002; 22:1199–1207. Available at: ISI:000174062300004. [PubMed: 11850447]

Parnavelas JG, Sullivan K, Lieberman AR, Webster KE. Neurons and Their Synaptic Organization in Visual-Cortex of Rat - Electron-Microscopy of Golgi Preparations. Cell Tissue Res. 1977; 183:499–517. Available at: ISI:A1977DZ70500006. [PubMed: 922850]

Povlishock JT, Kontos HA. Continuing axonal and vascular change following experimental brain trauma. Cent Nerv Syst Trauma. 1985; 2:285–298. [PubMed: 3836013]

Prince DA, Jacobs KM. Inhibitory function in two models of chronic epileptogenesis. Epilepsy Res. 1998; 32:83–92. Available at: http://www.ncbi.nlm.nih.gov/pubmed/9761311. [PubMed: 9761311]

Prince DA, Parada I, Scalise K, Graber K, Jin X, Shen F. Epilepsy following cortical injury: Cellular and molecular mechanisms as targets for potential prophylaxis. Epilepsia. 2009; 50:30–40. Available at: ISI:000262827500006. [PubMed: 19187292]

Prince DA, Tseng GF. Epileptogenesis in Chronically Injured Cortex - Invitro Studies. J Neurophysiol. 1993; 69:1276–1291. Available at: ISI:A1993KX59700024. [PubMed: 8492163]

Ravizza T, Gagliardi B, Noé F, Boer K, Aronica E, Vezzani A, Noe F. Innate and adaptive immunity during epileptogenesis and spontaneous seizures: evidence from experimental models and human temporal lobe epilepsy. NeurobiolDis. 2008; 29:142–160. Available at: http://www.ncbi.nlm.nih.gov/pubmed/17931873.

Salin P, Tseng GF, Hoffman S, Parada I, Prince DA. Axonal sprouting in layer V pyramidal neurons of chronically injured cerebral cortex. J Neurosci. 1995; 15:8234–8245. Available at: http://www.jneurosci.org/cgi/content/abstract/15/12/8234. [PubMed: 8613757]

Salin PA, Bullier J. Corticocortical connections in the visual system: structure and function. Physiol Rev. 1995; 75:107–154. Available at: ISI:A1995QB54900005. [PubMed: 7831395]

Schubert D, Staiger JF, Cho N, Kotter R, Zilles K, Luhmann HJ. Layer-specific intracolumnar and transcolumnar functional connectivity of layer V pyramidal cells in rat barrel cortex. J Neurosci. 2001; 21:3580–3592. Available at: ISI:000168409400033. [PubMed: 11331387]

Seiffert E, Dreier JP, Ivens S, Bechmann I, Tomkins O, Heinemann U, Friedman A. Lasting blood-brain barrier disruption induces epileptic focus in the rat somatosensory cortex. J Neurosci. 2004; 24:7829–7836. Available at: http://www.ncbi.nlm.nih.gov/pubmed/15356194. [PubMed: 15356194]

Shepherd GMG, Pologruto TA, Svoboda K. Circuit analysis of experience-dependent plasticity in the developing rat barrel cortex. Neuron. 2003; 38:277–289. Available at: http://www.ncbi.nlm.nih.gov/pubmed/12718861. [PubMed: 12718861]

Smeal RM, Keefe KA, Wilcox KS. Differences in excitatory transmission between thalamic and cortical afferents to single spiny efferent neurons of rat dorsal striatum. Eur J Neurosci. 2008; 28:2041–2052. Available at: http://www.pubmedcentral.nih.gov/articlerender.fcgi?artid=2596669&tool=pmcentrez&rendertype=abstract. [PubMed: 19046385]

Spruston N. Pyramidal neurons: dendritic structure and synaptic integration. Nat Rev Neurosci. 2008; 9:206–221. Available at: http://www.ncbi.nlm.nih.gov/pubmed/18270515. [PubMed: 18270515]

Spruston N, Jaffe DB, Williams SH, Johnston D. Voltage-Clamp and Space-Clamp Errors Associated with the Measurement of Electrotonically Remote Synaptic Events. J Neurophysiol. 1993; 70:781–802. Available at: ISI:A1993LU33100028. [PubMed: 8410172]

Taniguchi N, Takada N, Kimura F, Tsumoto T. Actions of brain-derived neurotrophic factor on evoked and spontaneous EPSCs dissociate with maturation of neurones cultured from rat visual cortex. J Physiol. 2000; 527(Pt 3):579–592. Available at: http://www.pubmedcentral.nih.gov/articlerender.fcgi?artid=2270088&tool=pmcentrez&rendertype=abstract. [PubMed: 10990542]

Topolnik L, Steriade M, Timofeev I. Partial cortical deafferentation promotes development of paroxysmal activity. Cereb Cortex. 2003a; 13:883–893. Available at: ISI:000184399800010. [PubMed: 12853375]

Topolnik L, Steriade M, Timofeev I. Hyperexcitability of intact neurons underlies acute development of trauma-related electrographic seizures in cats in vivo. Eur J Neurosci. 2003b; 18:486–496. Available at: http://doi.wiley.com/10.1046/j.1460-9568.2003.02742.x. [PubMed: 12911745]

Author Manuscript Author Manuscript Author Manuscript Author Manuscript

Tseng GF, Prince DA. Structural and functional alterations in rat corticospinal neurons after axotomy. J Neurophysiol. 1996; 75:248–267. Available at: http://www.ncbi.nlm.nih.gov/pubmed/8822555. [PubMed: 8822555]

Ulrich D, Luscher HR. Miniature Excitatory Synaptic Currents Corrected for Dendritic Cable Properties Reveal Quantal Size and Variance. J Neurophysiol. 1993; 69:1769–1773. Available at: ISI:A1993LD03600032. [PubMed: 8389839]

Vezzani A, Balosso S, Ravizza T. The role of cytokines in the pathophysiology of epilepsy. Brain Behav Immun. 2008; 22:797–803. Available at: http://www.ncbi.nlm.nih.gov/pubmed/18495419. [PubMed: 18495419]

Vezzani A, Granata T. Brain inflammation in epilepsy: experimental and clinical evidence. Epilepsia. 2005; 46:1724–1743. Available at: http://www.ncbi.nlm.nih.gov/pubmed/16302852. [PubMed: 16302852]

Vezzani A, Moneta D, Conti M, Richichi C, Ravizza T, De Luigi A, De Simoni MG, Sperk G, Andell-Jonsson S, Lundkvist J, Iverfeldt K, Bartfai T. Powerful anticonvulsant action of IL-1 receptor antagonist on intracerebral injection and astrocytic overexpression in mice. Proc Natl Acad Sci U S A. 2000; 97:11534–11539. [PubMed: 11016948]

Williams SR, Mitchell SJ. Direct measurement of somatic voltage clamp errors in central neurons. Nat Neurosci. 2008; 11:790–798. Available at: ISI:000257089400016. [PubMed: 18552844]

Williams SR, Stuart GJ. Dependence of EPSP efficacy on synapse location in neocortical pyramidal neurons. Science. 2002; 295:1907–1910. Available at: http://www.ncbi.nlm.nih.gov/pubmed/11884759. [PubMed: 11884759]

Williams SR, Stuart GJ. Role of dendritic synapse location in the control of action potential output. Trends Neurosci. 2003; 26:147–154. Available at: ISI:000181351900008. [PubMed: 12591217]

Yamamoto T, Nguyen TT, Stevens RT, Meiri KF, Hodge CJ. Increase of GAP-43 expression following kainic acid injection into whisker barrel cortex. Neuroreport. 2000; 11:1603–1605. Available at: ISI:000087375100002. [PubMed: 10852209]

Yang L, Afroz S, Michelson HB, Goodman JH, Valsamis HA, Ling DSF. Spontaneous Epileptiform Activity in Rat Neocortex after Controlled Cortical Impact Injury. J Neurotrauma. 2010; 27:1541–1548. Available at: ISI:000280984900017. [PubMed: 20504156]

Yang L, Benardo LS. Epileptogenesis following neocortical trauma from two sources of disinhibition. J Neurophysiol. 1997; 78:2804–2810. Available at: ISI:A1997YG93900053. [PubMed: 9356429]

Yang L, Benardo LS, Valsamis H, Ling DS. Acute injury to superficial cortex leads to a decrease in synaptic inhibition and increase in excitation in neocortical layer V pyramidal cells. J Neurophysiol. 2007; 97:178–187. [PubMed: 16987927]

Author Manuscript Author Manuscript Author Manuscript Author Manuscript

Highlights

- GAP43/VGLUT1-IR colocalized in terminals around pyramidal (Pyr) somata in UC cortex
- Putative excitatory synapses (VGLUT1/PSD95 puncta) on layer V Pyr cell somata in UC
- Epileptiform bursting present in slices from isolated (UC) neocortex 3d after injury
- EPSC data and LSPS mapping experiments indicate new excitatory network connectivity
- Excitatory rewiring contributes to hyperexcitability and early seizures after TBI

Author Manuscript
Author Manuscript
Author Manuscript
Author Manuscript

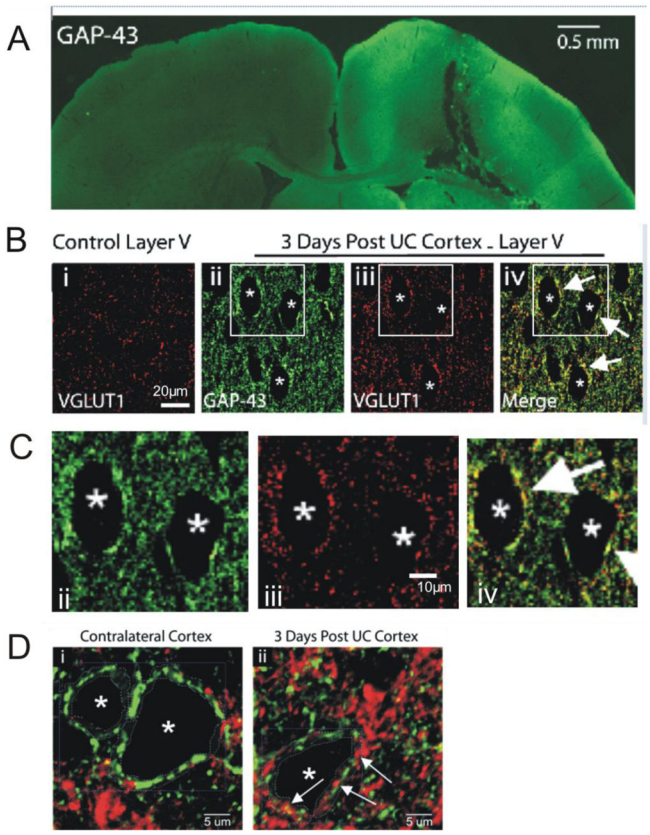

Figure 1.

New aberrant excitatory terminals are present in the UC cortex. **A.** Immunoreactivity (IR) for GAP-43 in lesioned cortex (green). Prominent IR is seen within the undercut and in the ipsilateral cortical and subcortical regions, but not in homotopic regions of uninjured contralateral cortex. Scale bar: 0.5 mm. **B.** Single plane layer V confocal images. Bi: Diffuse VGLUT1-IR in control cortex (red). Bii-Biii: GAP-43-IR and VGLUT1-IR from dual-reacted section of UC cortex. Perisomatic VGLUT1 puncta are more prominent in UC vs control (Bi vs Biii). Biv: Merged image of Bii and Biii shows some perisomatic close appositions of VGLUT1 and GAP-43 (white arrows). Asterisks mark the same 3 presumptive Pyr cells in Bii-Biv. Scale bar in Bi: 20 μm for Bi-iv. **C.** Enlarged images of B ii, iii, and iv to show colocalization of GAP43 and VGLUT1. Scale bar in Ciii for Cii-iv. **D.** Single plane confocal images of layer V pyramidal neurons (asterisks) in contralateral (i) and UC (ii) cortex processed for VGAT1 (green) and VGLUT1 (red) immunoreactivity. Arrows in Dii: examples of VGLUT1 positive puncta in the perisomatic region of a layer V Pyr neuron (asterisk). Scale bar in D: 5 μm.

Author Manuscript Author Manuscript Author Manuscript Author Manuscript

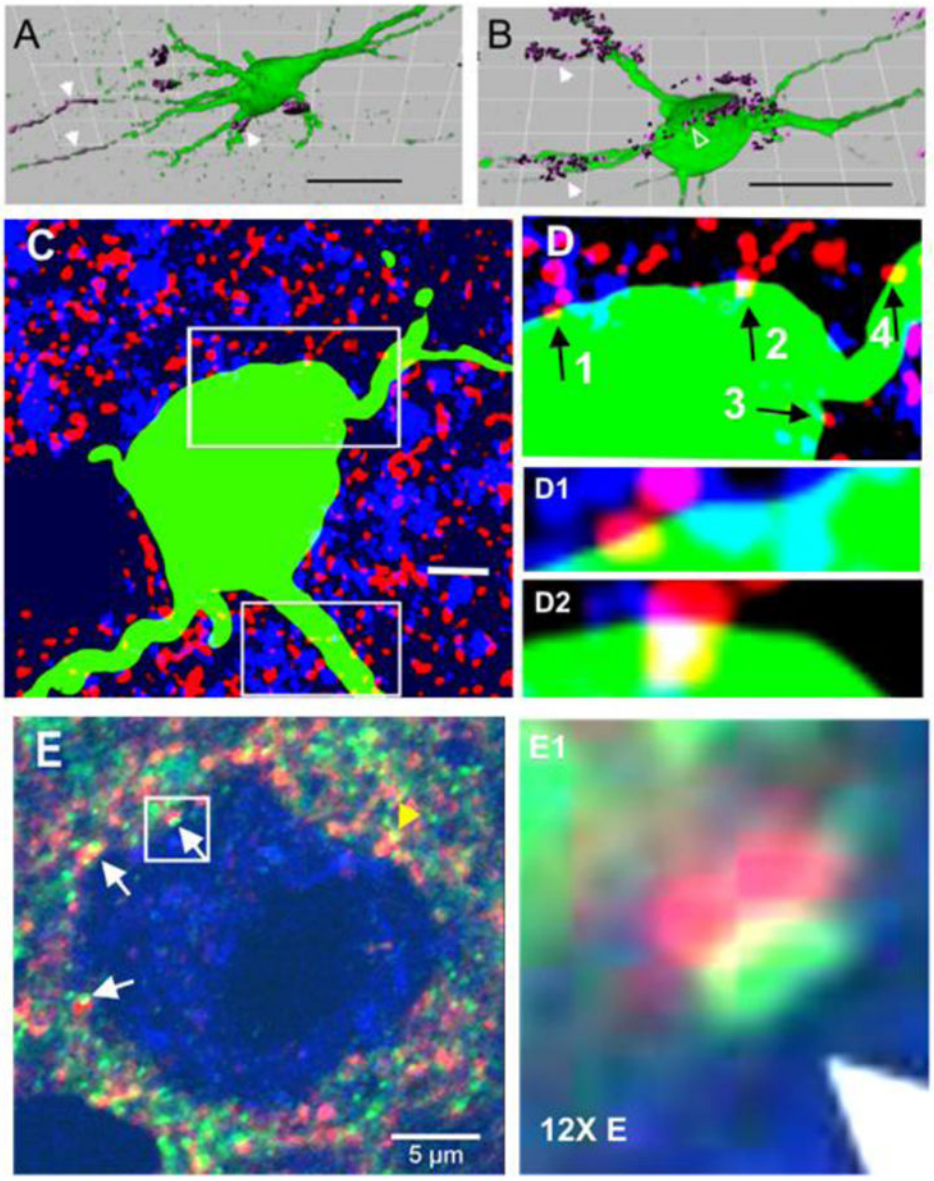

Figure 2.

Putative excitatory synapses on Pyr cell somata. **A:** Confocal image stack reconstruction (0.25 µm optical distance) of biocytin-filled control layer V pyramidal neuron (green). Section processed with antibodies for VGLUT1 and PSD95 such that dual co-immunoreactivity, selected by Volocity software, is magenta. White arrowheads point to sites of closely apposed VGLUT1- and PSD95-IR along basilar dendrites. **B:** Biocytin-filled layer V pyramidal cell from cortex 3d after undercut, reconstructed as in cell of A. Voxels of VGLUT1/PSD95 (magenta) in close apposition on basal dendrites (white arrowheads) and soma (open arrow) are indicated and were confirmed during cell rotation (Methods and Fig. S1). In A and B, only VGLUT1/PSD95-IR in close apposition to green cell is labeled magenta. **C:** A biocytin-labeled layer V pyramidal cell (green) from 3d undercut cortex. Two adjacent images (optical distance 0.5 µm) were obtained through the center of the cell body

Author Manuscript Author Manuscript Author Manuscript Author Manuscript

and collapsed. VGLUT1- (red) and PSD95-IR (blue) are also shown. Black void (lower right) corresponds to soma of adjacent unfilled cell. Lower white rectangle: proximal apical dendrite. **D:** Enlarged image of portion of soma and basal dendrite within the upper white rectangle of C. Black arrows point to sites of close apposition of VGLUT1/PSD95-IR on soma (arrows 1–3) and dendrite (arrow 4). D1, D2: Enlarged areas of close apposition (presumptive synapses) indicated by arrows 1 and 2 in D, respectively. Calibration: in A and B: 50 μm; in C: 10 μm. Green: biocytin; red: VGLUT1; blue: PSD95. **E:** 1.0 μm optical section cut through the soma of a layer V pyramidal cell from a P21, 3 day UC rat perfused with 4% paraformaldehyde and reacted for PSD95 (green), VGLUT1 (red) and NeuN (blue soma). White arrows: colocalization (yellow spots) of post-synaptic PSD95 and presynaptic VGLUT1 on the soma at presumptive excitatory synapses. Yellow arrowhead upper right: VGLUT1 and PSD95 colocalization in neuropil. **E1:** Enlargement of area in white box of E ~12.5x showing presumptive synapse. Calibration bar: 5 μm. Cells from undercut and naïve control perfusion-fixed rats are shown in Fig. 3.

Author Manuscript Author Manuscript Author Manuscript Author Manuscript

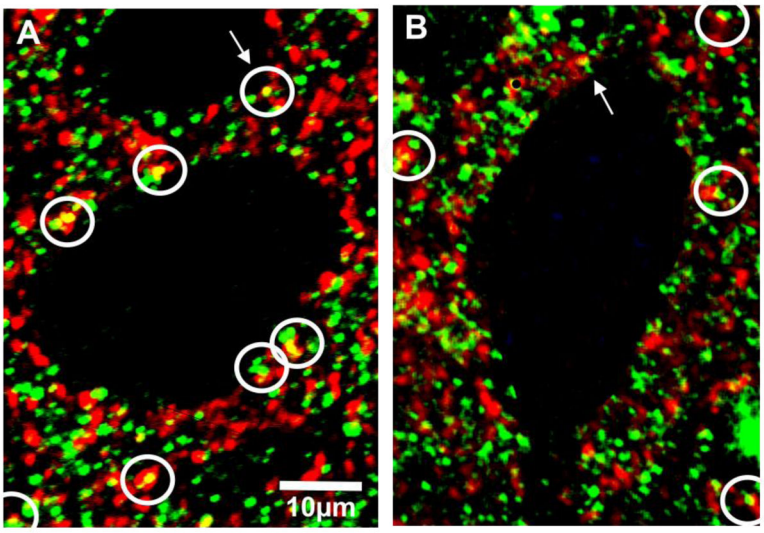

Figure 3.

VGLUT1/PSD95 close appositions on somata. **A:** Representative 1μm optical section through the soma of a layer V pyramidal cell from an undercut P21 rat perfused with 4% paraformaldehyde, and reacted for PSD95 (green), VGLUT1 (red) and NeuN (black soma). White circles: colocalization (yellow spots) of post-synaptic PSD95 and presynaptic VGLUT1 in the neuropil (bottom 2 circles) and at 4 presumptive excitatory somatic synapses. Arrow points to presumptive synapse on neighboring cell shown in ortho view in Fig. S2. **B.** Comparable section from control cell showing PSD95/VGLUT1 colocalizations are present in neuropil. White arrow points to rare possible synapse on soma (see Table 2). Apical dendrite down. Calibration in A for A–B

Author Manuscript Author Manuscript Author Manuscript Author Manuscript

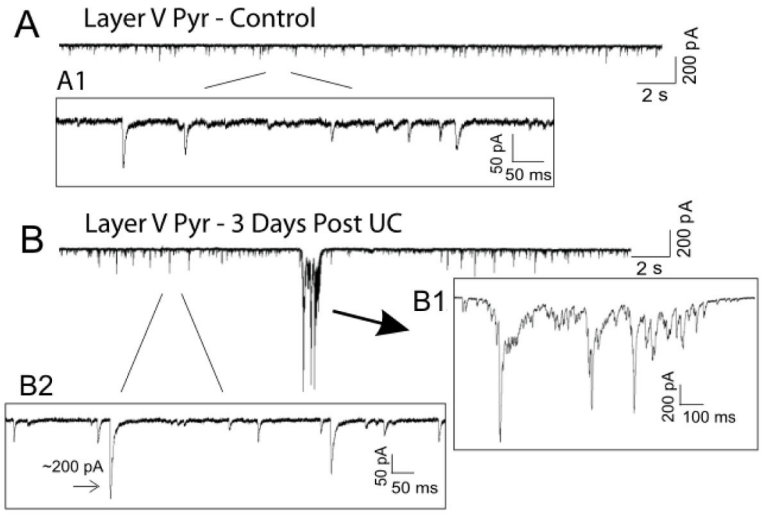

Figure 4.

Control data and spontaneous epileptiform bursts in whole-cell voltage clamp recordings from naive and UC slices. **A., A1**: Representative traces of whole cell recordings from layer V pyramidal (Pyr) neurons in slices from naïve control animals. A1: expanded segment of A showing spontaneous EPSCs. **B:** Whole cell recording from layer V Pyr cell 3 days post UC cortex. **B1** inset: expanded epileptiform burst from B. **B2:** expanded portion of B showing spontaneous EPSCs at expanded time scale and an example of a fast and large amplitude spontaneous EPSC (marked by arrow). Calibration: 200 pA, 2 sec for unexpanded control and 3 day post undercut traces.

Author Manuscript Author Manuscript Author Manuscript Author Manuscript

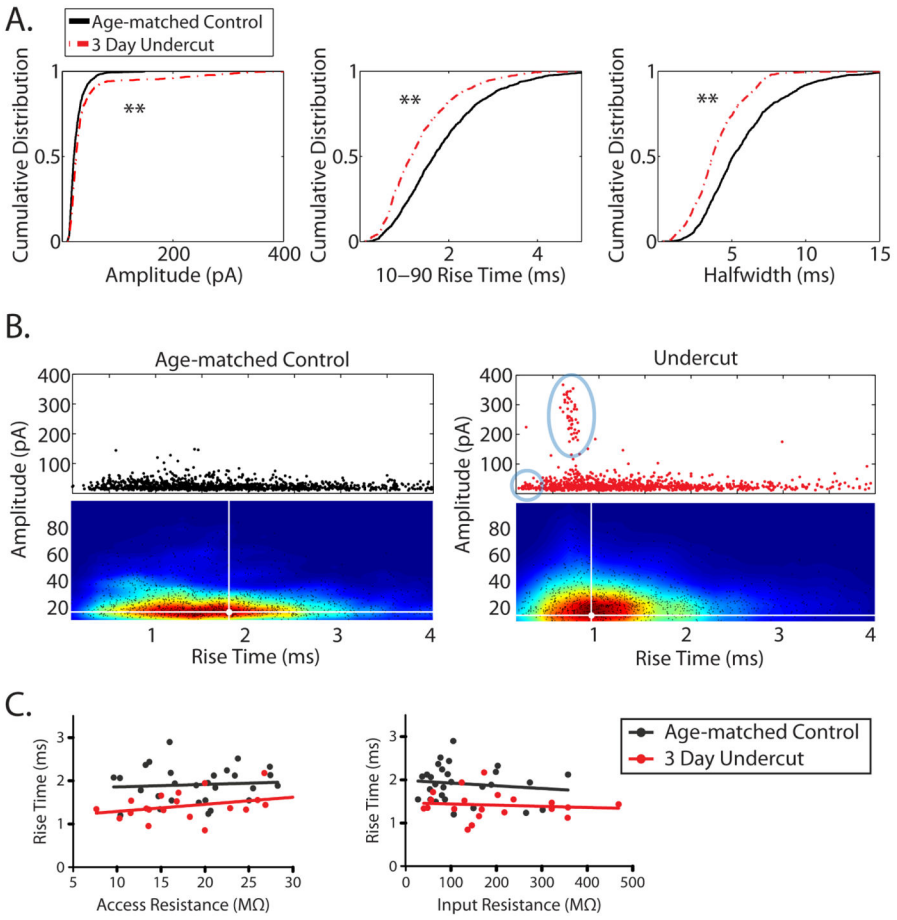

Figure 5.

Spontaneous EPSCs are faster and larger after UC. **A.** Cumulative distributions of peak amplitudes (left), 10–90 rise times (middle), and half-widths (right) of spontaneous EPSCs recorded from layer V pyramidal neurons in cortical slices from control (n = 29, black solid line) and UC (n = 23, red dashed line). **P < 0.0001, KS-test. **B.** Scatter plot and cloud density analysis (i.e. density heat maps) of sEPSC amplitude vs. rise time from control (left) and UC (right) slices. Responses in blue circle and oval represent populations of large and/or fast EPSCs not present in recordings from control slices. Peak of the density data is shown by the white dot and crosshair. Density of the data is represented by color in the heat maps; blue to red represents low to high density. C. Comparison of average rise time to access resistance (left) or input resistance (right) recorded from each cell in cortical slices from control (black dots) or undercut (red dots) animals.

Author Manuscript Author Manuscript Author Manuscript Author Manuscript

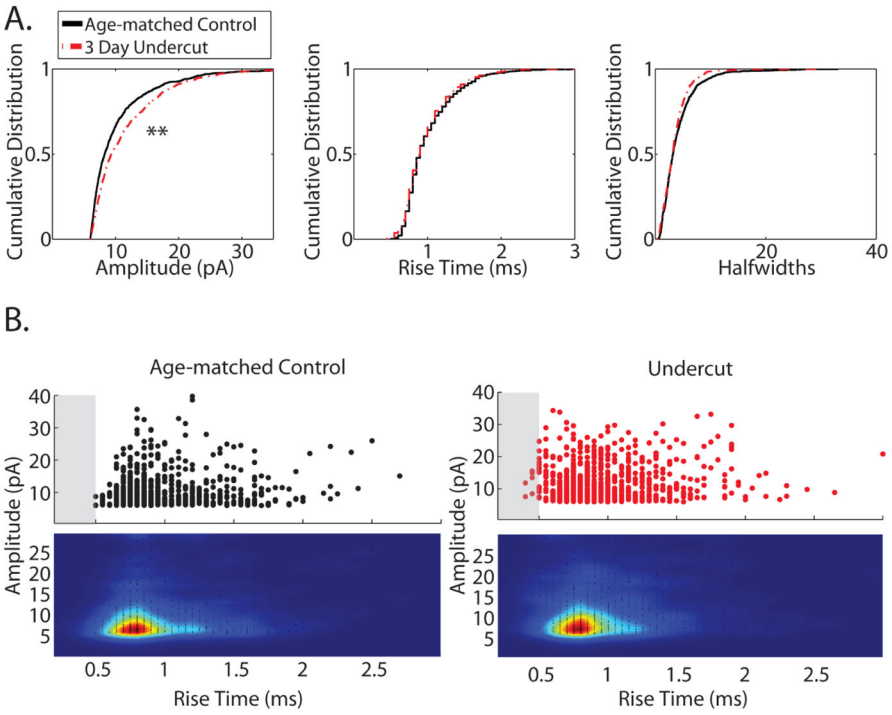

Figure 6.

Miniature (m) EPSC kinetics and amplitudes in slices from control and UC cortex. **A.** Cumulative distributions of peak amplitudes (left), 10–90 rise times (middle), and half widths (right) of mEPSCs recorded in the presence of 1 μM TTX from layer V pyramidal neurons in control (n = 10, black solid line) and UC (n = 11, red dashed line) slices. Peak amplitudes were larger in UC slices (d = 0.13, **P < 0.001), while rise times and half widths were not statistically different. **B.** Scatter plot and cloud density analysis of mEPSC amplitude vs. rise time from control (left) and UC (right) slices. Shaded boxes from 0 ms to 0.5 ms highlight a population of mEPSCs with fast rise times and larger amplitudes from UC slices not present in control slices

Author Manuscript Author Manuscript Author Manuscript Author Manuscript

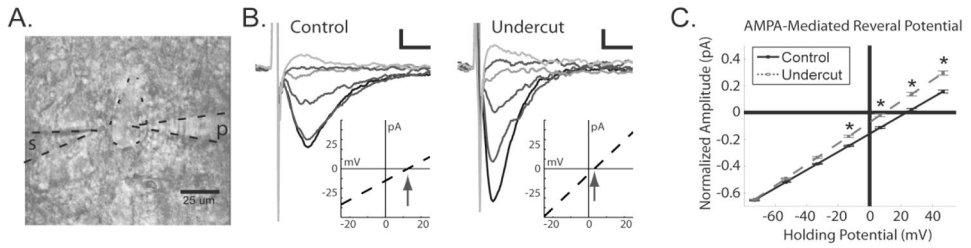

Figure 7.

AMPA-mediated reversal potentials are negatively shifted after UC. **A.** Example of the recording set-up. s: theta glass stimulating electrode placed ~20 away from the soma of the recorded cell (cell shown by outline in middle). p: patch pipette recording from a layer V pyramidal cell. **B.** Representative evoked currents in layer V Pyr cells at holding potentials from −73 mV to + 26 mV in incremental steps of 20 mV from control (left) and UC (right) cortex. Inset shows IV relationship for each cell, arrows point to reversal potential. Scale bar: 20pA/5ms. **C.** Average current-voltage relationships and reversal potentials from control (black solid line) and UC slices (gray dashed line). Note the negatively shifted reversal potential in recordings from UC slices. (*P < 0.05).

Author Manuscript Author Manuscript Author Manuscript Author Manuscript

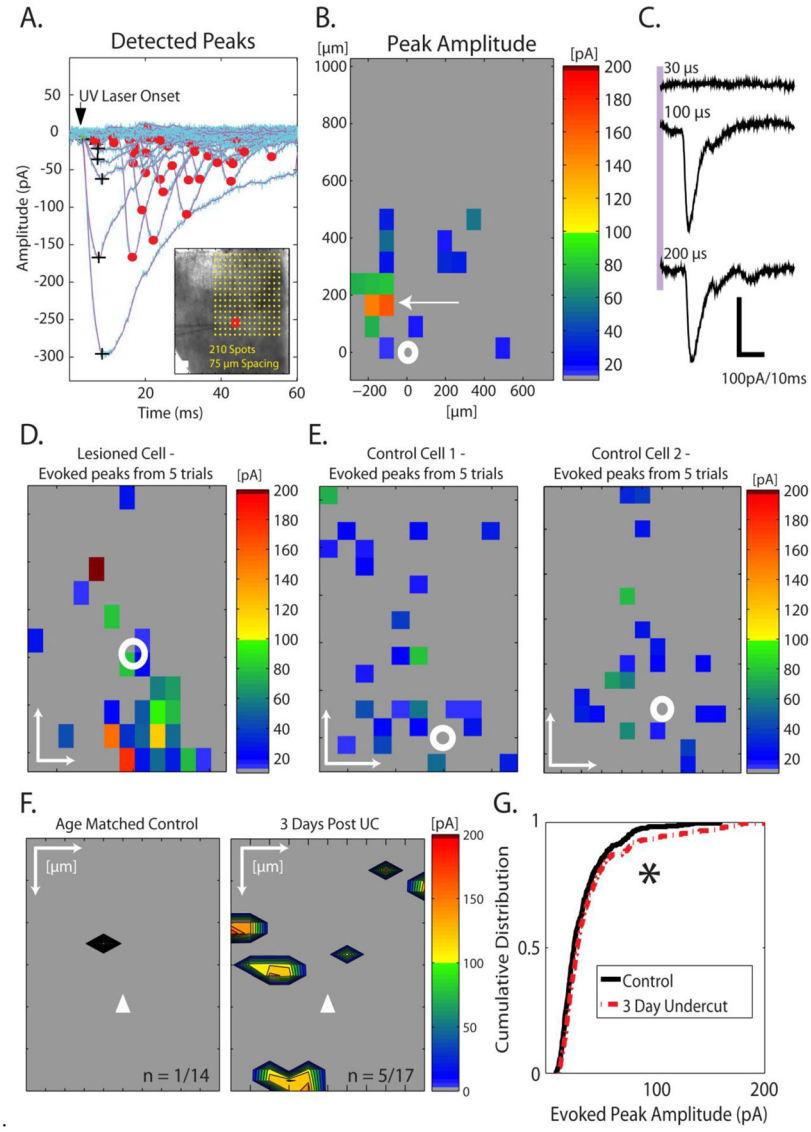

Figure 8.

Focal glutamate uncaging evokes large amplitude EPSCs after UC. **A.** LSPS-evoked currents were segregated as either direct responses (black +) that resulted from glutamate uncaged onto the neuron being recorded, or putative monosynaptic events (red circles on peaks) from synaptically connected presynaptic neuron(s) depolarized to threshold by glutamate uncaging. The various latencies of monosynaptic EPSCs presumably represent variable latency to reach threshold in stimulated presynaptic neurons. Inset: DIC image of recorded UC slice from experiment in (A) with respect to laser scanning photostimulation locations. Yellow dots in inset: locations of laser evoked glutamate uncaging. Red circle: position of the recorded cell in layer V of UC neocortex. Pial surface is up here and in B, D–F. **B.** Single trial heat map that shows the peak amplitude of putative monosynaptic EPSCs recorded in (A) in response to glutamate uncaging at the locations shown in inset of (A). White circle: location of recorded cell in layer V; white arrow: one location from which a single large amplitude EPSC was evoked. **C.** The large amplitude EPSC evoked from the location

Author Manuscript Author Manuscript Author Manuscript Author Manuscript

indicated by arrow in (B) appeared to be all-or-none as it was triggered abruptly at threshold and its amplitude and latency were insensitive to doubling of the duration of the laser pulse (laser onset indicated by purple vertical bar). Similar all-or-none EPSCs were elicited in 4 neurons where they could be repeatedly evoked by laser flashes. **D.** Heat map constructed from averaging 5 trials from a Pyr cell in a different UC slice. Note the amplitude scale and the evoked monosynaptic EPSCs with peak amplitudes >100 pA. **E.** Two examples of averaged maps from control cells (5 maps from each cell). In D and E, white scale bars: 200 μm for both X and Y axes, white circle: location of recorded cell in layer V. Identical heat map scale bars are used in B, D, and E. **F.** Averaged maps from multiple trials showing the locations from which large amplitude EPSCs (>100 pA) could be evoked in control cortical slices (left map; n = 1 of 14 slices) and UC (right map; n = 5 of 17 slices). EPSCs <75 pA are not shown in these maps. Note the greater number of locations and laminar and columnar distributions from where large amplitude EPSCs were evoked in UC slices. Scale bars: 100 μm for X axis, 200 μm for Y axis. White triangle: location of recorded cell in layer V. G. Cumulative distribution of uncaging-evoked EPSCs from all cells shows a significant shift for larger amplitude EPSCs in UC vs. control slices (*P < 0.5).

Author Manuscript

Author Manuscript

Author Manuscript

Author Manuscript

Table 1

Colocalization of VGLUT1 and PSD95-IR in perisomatic region (volume) of interest for biocytin-filled layer V pyramidal cells

Cell number	ROI Volume (μm^3)	VGLUT1 + PSD95 Colocalization Volume (μm^3)	Colocalization %
CNTRL Cell 1	293	0	0
CNTRL Cell 2	320	0	0
CNTRL Cell 3	283	0	0
CNTRL Cell 4	279	0	0
CNTRL Cell 5	289	0	0
Mean ± SEM	292.80 ± 7.21	0	0
UC Cell 1	283	7.73	2.72
UC Cell 2	272	7.77	2.85
UC Cell 3	228	5.55	2.55
UC Cell 4	222	6.17	2.78
UC Cell 5	293	7.82	2.76
UC Cell 6	289	9.11	3.2
UC Cell 7	273	8.78	3.21
Mean ± SEM	265.71 ± 10.92	7.56 ± 0.49	2.87 ± 0.10
p-value	0.09	4.57E-06	8.17E-08

CNTRL: control; UC: undercut; ROI: perisomatic volume of interest

Author Manuscript Author Manuscript Author Manuscript Author Manuscript

Table 2

Visually Identified Putative Somatic Synapses

Rat #	# cells analyzed	Count of synapses/cell									
Undercut 1	10	3	2	3	2	3	4	4	3	2	3
Undercut 2	10	2	3	3	5	3	4	3	3	2	3
Undercut 3	10	2	5	3	3	4	2	3	2	3	2
Control 1	10	1	0	0	0	0	0	0	0	0	0
Control 2	10	1	0	0	0	0	0	0	0	0	0
Control 3	10	0	0	0	0	0	0	0	0	0	0

Mean synapses ± SEM in UC and control: 2.97 ± 0.16 N=30 and 0.07 ± 0.05 N=30, respectively, unpaired t test: P<0.0001

Author Manuscript

Author Manuscript

Author Manuscript

Author Manuscript

Table 3

Amplitude and kinetics of sEPSCs

Parameter	Control (n=29)	Undercut (n=23)	P- value
Amplitude (pA)	24.9 ± 1.2	38.2 ± 6.5*	< 0.02
Rise Time (ms)	1.89 ± 0.08	1.39 ± 0.07****	< 0.0001
Halfwidth (ms)	5.84 ± 0.32	4.19 ± 0.28***	< 0.001
Total Charge (fC)	152.3 ± 10.7	185.6 ± 42.8	> 0.5

All data are expressed as mean ± SEM. Significance tested by Student's t-test

Author Manuscript

Author Manuscript

Author Manuscript

Author Manuscript

Table 4

Amplitude and kinetics of mEPSCs

Parameter	Control (n=11)	Undercut (n=10)	P- value
mEPSC Amplitude (pA)	10.14 ± 0.75	11.62 ± 0.43	> 0.13
mEPSC Rise Time (ms)	1.04 ± 0.03	1.14 ± 0.08	> 0.21
mEPSC Halfwidth (ms)	4.74 ± 0.38	3.57 ± 0.38	> 0.11

All data are expressed as mean ± SEM. Significance tested by Student's t-test